

# Dimensional transmutation from non-Hermiticity

Hui Jiang<sup>1,\*</sup> and Ching Hua Lee<sup>1,†</sup>

<sup>1</sup>*Department of Physics, National University of Singapore, Singapore 117551, Republic of Singapore*

(Dated: July 20, 2022)

Dimensionality plays a fundamental role in the classification of novel phases and their responses. In generic lattices of 2D and beyond, however, we found that non-Hermitian couplings do not merely distort the Brillouin zone (BZ), but can in fact alter its effective dimensionality. This is due to the fundamental non-commutativity of multi-dimensional non-Hermitian pumping, which obstructs the usual formation of a generalized complex BZ. As such, basis states are forced to assume “entangled” profiles that are orthogonal in a lower dimensional effective BZ, completely divorced from any vestige of lattice Bloch states unlike conventional skin states. Characterizing this reduced dimensionality is an emergent winding number intimately related to the homotopy of non-contractible spectral paths. We illustrate this dimensional transmutation through a 2D model whose topological zero modes are protected by a 1D, not 2D, topological invariant. Our findings can be readily demonstrated via the bulk properties of non-reciprocally coupled platforms such as circuit arrays, and provokes us to rethink about the fundamental role of geometric obstruction in the dimensional classification of topological states.

*Introduction.*— Dimensionality is fundamental in determining possible physical phenomena. At the cosmological level, our (3+1)-D space-time have constrained possible gravitational and string theories [1–4]. In field theory, the rich conformal symmetry in 2D has led to great advancements in percolation theory and quantum entanglement [5–14]. Condensed matter phenomena are also intimately tied to dimensionality, such as the scaling of heat capacities [15], Anderson localization [16–18] and critical phase transitions [19, 20]. In particular, symmetry-protected topological phases can be systematically classified based on Bott periodicity in the number of dimensions, via the tenfold-way [21–27]. More recently, this classification has been greatly enriched [28–33] by including non-Hermitian lattices, which are increasingly studied both theoretically [34–54] and in photonic, mechanical, electrical and cold-atom experiments [55–75].

Usually, it is taken for granted that the dimensionality of the topological invariant [76–82] coincides with that of the physical space. This is because they are defined in reciprocal (momentum) space, which should be of the same dimension as the physical lattice, at least in Euclidean space[83]. Even amongst enigmatic non-Hermitian phenomena featured lately, where the band structure and topological invariants are substantially modified by boundaries and impurities [84–106], the highly distorted effective Brillouin zone (BZ) is still indexed by states living in the same dimensionality.

Yet we discover, surprisingly, that in 2D and beyond, non-Hermiticity can in fact *change* the effective BZ dimensionality. This holds true for generic non-Hermitian lattices beyond the simplest monoclinic structures, whenever the lattice is bounded (as all realistic lattices should be). Hence, the effective band structure of a  $D$ -dim lattice may in reality live in  $D' < D$  dimensions, and be classified by  $D'$  instead of  $D$ -dim topology.

Underlying this dimensional transmutation is a hith-

erto unnoticed geometric obstruction. Concretely, it manifests as the non-commutativity in the equilibration of non-Hermitian pumped states along different directions. Fundamentally resulting from emergent non-locality [107][84, 108], it is reminiscent of the non-commutativity of magnetic translations due to the non-locality of flux threading, as epitomized by the Aharonov-Bohm effect [109–111]. Below, we shall demonstrate the necessity of dimensional transmutation through concrete examples, and show how the effective BZ manifold can be constructed from homotopy loops in the original BZ that avoid the non-commutativity.

*Non-Hermitian equilibration and its non-commutativity.*— We first review the equilibration of non-Hermitian pumping, and reveal how its non-commutative nature can fundamentally alter the momentum-space lattice (the BZ), including its dimensionality. Consider a generic lattice under open boundary conditions (OBCs)

$$H = \sum_{\mathbf{x};\alpha,\beta} \sum_{\{\mathbf{e}\}} h_{\mathbf{e}}^{\alpha\beta} c_{\mathbf{x}+\mathbf{e},\alpha}^{\dagger} c_{\mathbf{x},\beta}, \quad (1)$$

where  $\mathbf{e}$  ranges over all coupling displacements from each unit cell, and  $\alpha, \beta$  are sublattice component indices. When the couplings have asymmetric amplitudes  $|h_{\mathbf{e}}^{\alpha\beta}| \neq |h_{-\mathbf{e}}^{\beta\alpha}|$ , which can physically arise from the combination of flux and gain or loss, all left/right moving states are invariably attenuated/amplified by a factor of  $|h_{\mathbf{e}}^{\alpha\beta}|/|h_{-\mathbf{e}}^{\beta\alpha}|$  per unit cell shifted [112–114]. This leads to a dramatic density accumulation of “non-Hermitian pumped” states at lattice boundaries or impurities. When it is just simple exponential build-up, they are represented by non-Hermitian skin effect (NHSE) eigenstates; in more esoteric critical cases, they can assume special scale-free eigenstate profiles [97, 115–119]. In generic higher-dimensional lattices that this work focuses on, such boundary accumulations have not been properly characterized.

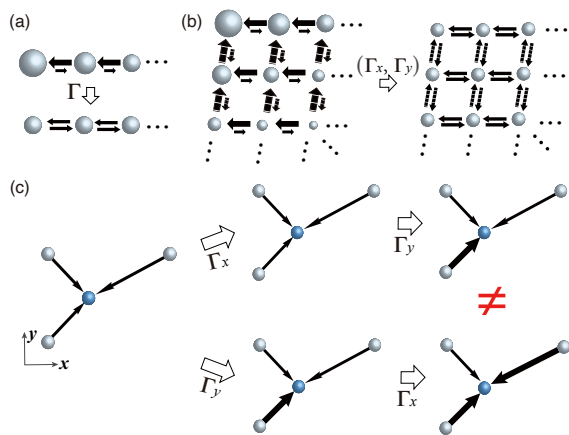


FIG. 1. a) To obtain the effective BZ of a 1D lattice, all couplings can always be symmetrized through a straightforward equilibration  $\Gamma$ . b) Higher-dimensional “unentangled” lattices can still be similarly symmetrized via independent equilibrations  $\Gamma_x, \Gamma_y, \dots$  c) Generic “entangled” lattices of 2D and beyond cannot be completely equilibrated, since equilibrations  $\Gamma_j$  do not commute in general; shown is a minimal example where  $\Gamma_x \Gamma_y \neq \Gamma_y \Gamma_x$ , i.e. where symmetrization in one direction can un-symmetrize the coupling components in the other direction (arrow thickness depict coupling strength). Hence obtaining the effective BZ through naive NHSE-inspired equilibration is doomed to failure.

Since the Bloch eigenstates that define the original BZ are highly distorted by non-Hermitian pumping, all “bulk” properties such as band topology, transport and geometry will be radically modified. To correctly characterize them, it is necessary to construct the effective BZ where the spatially non-uniform pumped eigenstates are “equilibrated” to approximately resemble Bloch states [91, 108]. The simplest illustrative example, well-known in the NHSE literature, is the 1D “Hatano-Nelson” chain with asymmetric nearest-neighbor couplings  $h_{\pm\hat{x}} = he^{\mp\kappa}$  (Fig. 1a) [94, 112–114]. Under OBCs, its eigenstates assume the boundary-localized form  $\psi_{\text{HN}}(x) \sim e^{-\kappa x}$ , which can be “equilibrated” into the bulk through a basis rescaling operator  $\Gamma$ :  $c_x^\dagger \rightarrow e^{\kappa x} c_x^\dagger$ ,  $c_x \rightarrow e^{-\kappa x} c_x$ . At the same time,  $\Gamma$  also “balances” the equilibrated couplings, as shown in Fig. 1a, as well as induce an effective complex deformed BZ viz.  $c_k^\dagger = \sum_x e^{ikx} c_x^\dagger \rightarrow \sum_x e^{i(k-i\kappa)x} c_x^\dagger = \sum_x z(k)^x c_x^\dagger$  where  $-i \log z(k) = k - i\kappa$  is the complexified momentum. In higher-dimensional lattices that can be decomposed into “unentangled” 1D chains i.e. a simple monoclinic 2D lattice (Fig. 1b), one can analogously apply an equilibration operator  $\Gamma_j$  whenever OBCs are taken along the  $j$ -th direction.

For most generic lattices in 2D or higher, however, this NHSE-inspired equilibration procedure fails to give the correct equilibrated lattice couplings and hence effective BZ. Consider the minimal model illustrated in Fig. 1c, with three non-orthogonal asymmetric hoppings

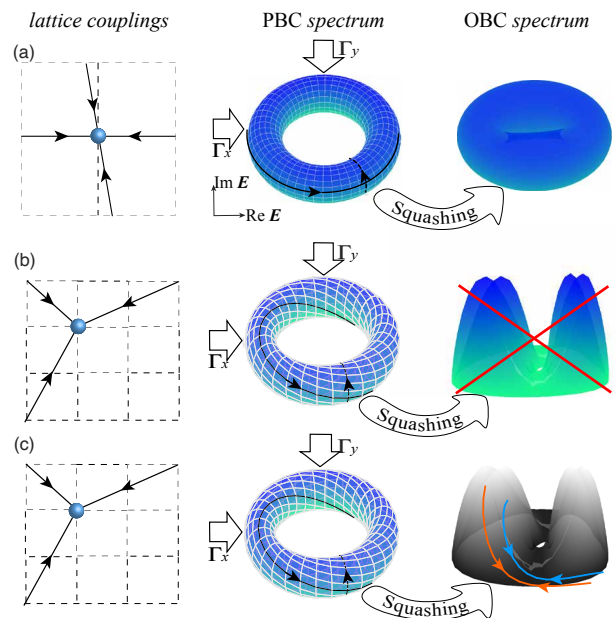


FIG. 2. a) An “unentangled” lattice admits fully commuting equilibration operators  $\Gamma_x, \Gamma_y$  that completely “squashes” its PBC spectral torus  $E_{2D}$  into a “flattened” OBC torus  $\bar{E}_{2D}$ . b) An “entangled” lattice is subject to non-commuting equilibrations  $\Gamma_x \Gamma_y \Gamma_x^{-1} \Gamma_y^{-1} \neq \mathbb{I}$ , such that its PBC spectrum can no longer be completely “squashed” into a valid OBC spectrum with no spectral winding, akin to a filled balloon. c) The correct OBC spectrum of the “entangled” 2D lattice is traced out by 1D homotopy paths (blue, red) on the incompletely squashed spectral torus that avoid any spectral winding.

from each site that nontrivially “entangle” the two lattice directions. We would like to derive the boundary-accumulated eigenstates when the lattice (not explicitly shown) is under OBCs in both  $x$  and  $y$  directions. At each equilibration step  $\Gamma_j$ , the combined coupling strength component in the  $j$ -th direction are to be “balanced”: in Fig. 1c, the  $\Gamma_x$  operation modifies the original couplings negligibly because the x-components are already approximately equal, but not so for  $\Gamma_y$ . Importantly, we see that exchanging the order of performing the equilibrations  $\Gamma_x, \Gamma_y$  yield different equilibrated couplings, even though the effective lattice should of course *not* depend on the order in which the  $x, y$ -OBCs are taken. This non-commutativity of  $\Gamma_x$  and  $\Gamma_y$ , even for such a minimal example, suggests that physical states are pumped in a peculiar non-local manner, and an entirely new approach is needed for correctly characterizing the effective BZ whenever a multi-dimensional lattice cannot be trivially decoupled into 1D chains.

*Dimensional transmutation from non-commutative equilibration.*— We next show how multi-dimensional non-Hermitian pumping on the energy spectrum advocates an effective BZ of a different, lower dimension. Consider a 2D model given by  $H_{2D}(k_x, k_y)$  in momentum space. Under periodic boundary conditions (PBCs),

its energy spectrum  $E_{2D}(k_x, k_y)$  generically resembles a deformed torus projected onto a 2D plane (Fig. 2), since it takes complex values and is parametrized by two periodic momenta. Going from PBCs to OBCs, this spectrum  $E_{2D} \rightsquigarrow \bar{E}_{2D}$  must necessarily be “squashed” in the complex plane by non-Hermitian pumping, since it is known that under OBCs [120], any 1D subsystem i.e. any 1D loop traced by  $E_{2D}(k_x, k_y)$  with fixed  $k_x$  or  $k_y$  must be degenerate (enclosing zero area) in the complex energy plane:  $\oint \partial_{k_j} \log(\bar{E}_{2D}(\mathbf{k}) - E_0) dk_j = 0$  for all  $E_0 \in \mathbb{C}$ ,  $j = x, y$ .

However, the spectral squashing in 2D is often not straightforward like in 1D, where equilibration always amounts to a complex BZ deformation  $e^{ik} \rightarrow z(k) \rightarrow e^{i(k-i\kappa(k))}$  that completely squashes  $E_{1D}(k) \rightarrow E_{1D}(k)(k - i\kappa(k)) = \bar{E}_{1D}(k)$  into a degenerate spectral loop. As sketched in Fig. 2a for an “unentangled” 2D lattice,  $\Gamma_x$  and  $\Gamma_y$  is allowed to successively “squash” the spectral torus until it contains no non-degenerate loops, since the lattice trivially decouples into two non-parallel 1D chains. However, for an “entangled” 2D lattice (Fig. 2b,c),  $\Gamma_x \Gamma_y \Gamma_x^{-1} \Gamma_y^{-1} \neq \mathbb{I}$  and the “squashing” cannot be complete - picture a filled balloon which can be compressed in one direction, but not squashed in all directions simultaneously. As a result, the incompletely “squashed” spectral torus still contains nondegenerate loops, and the only solution is to exclude them from the effective BZ itself (Fig. 2c). In this case, the effective BZ can only be spanned by the homotopy generator independent from any nondegenerate spectral loop, and can only be of 1D despite the physical lattice being of 2D. Fig. 3a shows an example where successive application of  $\Gamma_x$  followed by  $\Gamma_y$  gives the incorrect spectrum (blue), different from the numerically obtained spectrum (red). As such, even though effective 1D BZs possess well-defined complex momenta viz.  $z(k) = e^{i(k-i\kappa(k))}$ , in 2D or higher,  $z_j(\mathbf{k}) \neq e^{i(k_j - i\kappa_j(\mathbf{k}))}$ ,  $j = x, y, \dots$  in general, defying the well-established NHSE framework.

*Construction of dimensionally transmuted effective BZ.* - Having explained why the effective BZ may have lower dimensionality than the physical lattice, we now demonstrate its concrete construction through a 1-component example of the type shown in Fig. 2b,c. We refer to it as the type-III model in our Supplement [121], where it was also explained why it but not related models undergo nontrivial dimensional transmutation:

$$H_{2D} = \sum_{\mathbf{x}} t_1 c_{\mathbf{x}}^{\dagger} c_{\mathbf{x} + \alpha \hat{x} + a \hat{y}} + t_2 c_{\mathbf{x}}^{\dagger} c_{\mathbf{x} - \beta \hat{x} + a \hat{y}} + t_3 c_{\mathbf{x}}^{\dagger} c_{\mathbf{x} - \beta \hat{x} - b \hat{y}}. \quad (2)$$

Applying the ansatz  $\psi_{2D}(x, y) \propto z_x^x z_y^y$  for an eigenstate, we obtain the energy relation

$$E_{2D}(z_x, z_y) = t_1 z_x^{\alpha} z_y^a + t_2 z_x^{-\beta} z_y^a + t_3 z_x^{-\beta} z_y^{-b}. \quad (3)$$

At this stage, no assumption is made about the boundary conditions, and the assertion is that  $E_{2D}(z_x, z_y)$  yields the correct eigenenergy given appropriate forms of  $z_x, z_y$ .

To correctly obtain the effective BZ from  $E_{2D}(z_x, z_y)$ , we would need to treat the effects of both  $x$  and  $y$ -OBCs on equal footing. This can be achieved by implementing the two OBCs one at a time, by considering the other momentum as a parameter. Given a quasi-1D energy function  $E_{1D}(z)$ , we determine the effective BZ by finding a complex effective momentum function  $-i \log z(k)$ ,  $k \in [0, 2\pi)$ , such that every energy eigenvalue  $E = E_{1D}(z(k))$  corresponds to at least two different  $k$  solutions with identical  $|z(k)|$  [85, 90]. In a trivial case without non-Hermitian pumping, we simply have  $z(k) = e^{ik}$ , such that the effective and original BZs coincide. In this work, we shall not delve into the intricacies of finding the effective BZ of various 1D models; rather, we just quote the new result relevant to our 2D example, as derived in our Supplement [121]: For  $E_{1D}(z) = Az^p + Bz^{-q}$  corresponding to left(right) hoppings over  $p$  ( $q$ ) sites, we have

$$z(k) = \left( \frac{B \sin qk}{A \sin pk} \right)^{\frac{1}{p+q}} e^{i \frac{2\pi\nu}{p+q} k} e^{ik} = e^{-\kappa_{1D}(k)} e^{ik}, \quad (4)$$

for  $k \in (-\pi/(p+q), \pi/(p+q)]$ ,  $\nu = 1, 2, \dots, p+q$  labeling the solution branch. The decay function  $e^{-\kappa_{1D}(k)}$  encodes how non-Hermitian pumping distorts the Bloch phase factor  $e^{ik}$ . Notice that the mapping  $e^{ik} \rightarrow z(k)$  is only piecewise-smooth - this non-analyticity stems from the non-locality of non-Hermitian pumping, even though the hopping processes are clearly local.

By applying Eq. 4 on  $z_x, z_y$  of Eq. 3 separately, we obtain  $z_x^{\alpha+\beta} = (t_2 + t_3 z_y^{-(\alpha+\beta)}) / (t_1 \sin \alpha k_1) \sin \beta k_1 e^{i(\alpha+\beta)k_1}$  and  $z_y^{-(\alpha+\beta)} = (t_2 + t_1 z_x^{\alpha+\beta}) / (t_3 \sin b k_2) \sin a k_2 e^{-i(\alpha+\beta)k_2}$ , where we have used the notation  $k_1, k_2$  instead of  $k_x, k_y$  to emphasize that they may no longer be conjugate momenta to the  $x, y$  coordinates. We can simultaneously solve these expressions to obtain

$$z_x^{\alpha+\beta} = \frac{t_2 (\sin a k_2 + e^{i(\alpha+\beta)k_2} \sin b k_2) e^{i(\alpha+\beta)k_1} \sin \beta k_1}{t_1 e^{i(\alpha+\beta)k_2} \sin \alpha k_1 \sin b k_2 - e^{i(\alpha+\beta)k_1} \sin \beta k_1 \sin a k_2}, \quad (5a)$$

$$z_y^{a+b} = \frac{t_3 e^{i(\alpha+\beta)k_2} \sin \alpha k_1 \sin b k_2 - e^{i(\alpha+\beta)k_1} \sin \beta k_1 \sin a k_2}{t_2 (\sin \alpha k_1 + e^{i(\alpha+\beta)k_1} \sin \beta k_1) \sin a k_2}. \quad (5b)$$

We reiterate a major distinction between the  $z_x, z_y$  above and the effective “generalized” BZ of NHSE systems: In the latter, the BZ is “generalized” in the sense that  $z_j$ ,  $j = x, y$  encapsulates complex momentum via  $-i \log z_j = k_j - i\kappa_j(\mathbf{k})$ , with  $\kappa_j(\mathbf{k})$  representing the complex deformation. But in Eqs. 5a, 5b,  $-i \log z_j$  manifestly do not correspond to any single well-defined complex momentum (recall that  $\psi_{2D}(x, y) \propto z_x^x z_y^y$ ). Even though  $k_1, k_2$  are the “momenta” associated with quasi-1D chains within  $H_{2D}$ , they are now “entangled”, as evident in the highly nonlinear functional form of Eqs. 5a, 5b.

Importantly, the  $z_x, z_y$  from Eqs. 5a and 5b still do *not* describe the correct effective BZ unless  $k_1, k_2$  are further

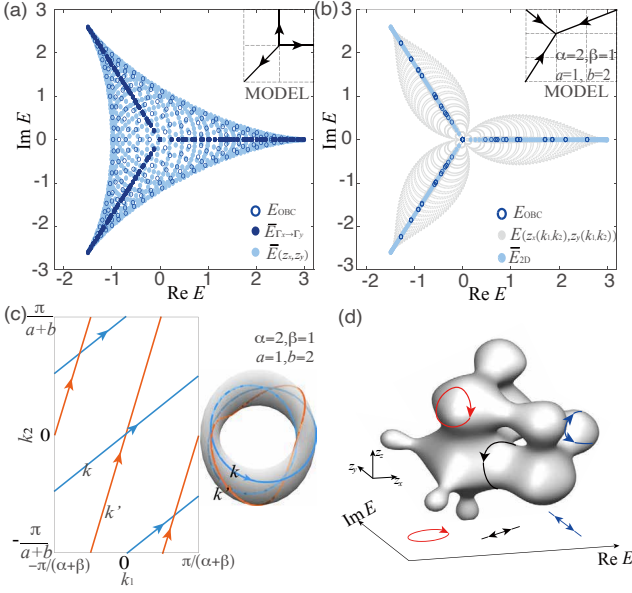


FIG. 3. a) Sequentially applying  $\Gamma_x$  and then  $\Gamma_y$  ( $x$ -OBCs and then  $y$ -OBCs) yields an incorrect OBC spectrum  $\bar{E}_{\Gamma_x \rightarrow \Gamma_y}$  (Dark blue) for the illustrative “entangled” 2D lattice  $H = \sum_{\mathbf{x}} c_{\mathbf{x}+\hat{x}}^\dagger c_{\mathbf{x}} + c_{\mathbf{x}+\hat{y}}^\dagger c_{\mathbf{x}} + c_{\mathbf{x}-\hat{x}-\hat{y}}^\dagger c_{\mathbf{x}}$ , at odds with the symmetrically obtained  $\bar{E}(z_x, z_y)$  (light blue), which reproduces the exact numerical  $E_{\text{OBC}}$  (blue circles). b) Necessity of dimensional transmutation of the BZ: For our model  $H_{2\text{D}}$  (Eq. 2), the effectively 1D  $\bar{E}_{2\text{D}}$  of Eq. 6 (light blue) agrees with the numerical  $E_{\text{OBC}}$  (blue circles), while the unconstrained  $E_{2\text{D}}$  from Eqs. 3 and 5a,5b gives extraneous eigenenergies (gray). c) The effective 1D BZ is given by the union of 1D winding paths (blue, red for  $k, k'$  respectively) on the  $k_1$ - $k_2$  2-torus. d)  $\mathcal{M}$  (gray blob) of an illustrative 3D model, with effective BZ given by its blue and black loops that correspond to degenerate spectral loops in the complex  $E$  plane below.

constrained, since we have not eliminated the possibility of  $E(z_x, z_y)$  exhibiting nontrivial windings as one of  $k_1$  or  $k_2$  is varied over a period [121]. Indeed, from Fig. 3b, naive substitution of the unconstrained  $z_x, z_y$  into Eq. 3 gives extraneous eigenenergies across the complex plane (gray), different from the numerical OBC spectrum (blue circles) which exhibits no spectral winding.

For our model, all spectral windings can be made to vanish along the two 1D parametrization paths  $(k_1, k_2) = (bk, \beta k)$  and  $(k_1, k_2) = (ak', \alpha k')$ , as rigorously shown in [121]. Indeed, in Fig. 3b, the union of these energies  $\bar{E}_{2\text{D}}(k) = E_{2\text{D}}(z_x(k), z_y(k))$  and  $\bar{E}'_{2\text{D}}(k') = E_{2\text{D}}(z'_x(k'), z'_y(k'))$  also agree with the numerical OBC spectrum. Their analytic expressions are given by

$$\begin{aligned}
 [\bar{E}'_{2\text{D}}(k')]^{\alpha+\beta} &= t_1^\beta t_2^{\frac{\alpha b - \beta a}{\alpha + \beta}} t_3^{\frac{a(\alpha + \beta)}{\alpha + \beta}} e^{2\pi i (a\nu \frac{\alpha + \beta}{\alpha + \beta} + \alpha\nu')} \\
 &\times \left( \frac{\sin(\alpha a + \beta a)k'}{\sin \alpha a k'} \right)^\alpha \left( \frac{\sin(\alpha a + \beta a)k'}{\sin \alpha a k'} \right)^{\frac{b(\alpha + \beta)}{\alpha + \beta}} \\
 &\times \left( \frac{\sin \alpha a k'}{\sin \beta a k'} \right)^\beta \left( \frac{\sin(\alpha b - \beta b)k'}{\sin \alpha a k'} \right)^{\frac{\beta a - \alpha b}{\alpha + \beta}}, \quad (6)
 \end{aligned}$$

and analogously for  $E_{2\text{D}}(k)$ . The union of the 1D loops described by  $k$  and  $k'$  forms the dimensionally transmuted effective BZ, as illustrated in Fig. 3c.

Interestingly, this effectively 1D BZ reveals a new avenue of topological winding, with winding numbers of  $\text{GCD}(a, \alpha)$  and  $\text{GCD}(b, \beta)$  describing how the sectors  $k'$  and  $k$  loop around the  $k_1$ - $k_2$  torus. (both windings are 2 in Fig. 3c). Physically,  $k_1, k_2$  represent the non-Bloch wavenumbers from separately taking OBCs in each direction; yet, when OBCs are simultaneously applied in both directions, the effective BZ collapses into closed 1D paths that mixes  $k_1$  and  $k_2$ . As such, these winding numbers encapsulate the amount of “entanglement” caused by 2-dimensional non-Hermitian pumping.

*Generalizations.*— We now generalize the construction of the dimensionally-transmuted effective BZ from our particular  $H_{2\text{D}}$  lattice to a generic model  $H$  in  $D$  dimensions. First, acting on the ansatz eigenstate  $\psi_D(\mathbf{x}) \propto \prod_j^D z_j^{x_j}$ , we express the model as a multivariate polynomial  $E(\mathbf{z}) = \sum_\mu t_\mu \prod_j z_j^{l_{\mu j}}$ , where  $l_{\mu j}$  is the range of the  $\mu$ -th hopping  $t_\mu$  in the  $j$ -th direction. Next, we apply the  $D$  equilibrations  $\Gamma_j, j = 1, \dots, D$  separately on  $E(\mathbf{z})$ , such that each becomes a quasi-1D problem in  $z_j$ , with all the components of  $\tilde{\mathbf{z}} = (z_1, \dots, z_{j-1}, z_{j+1}, \dots, z_D)$  as spectator parameters. Solving for the effective 1D BZs for each of them [90, 106, 108, 121] i.e. replacing each  $z_j$  by appropriate  $e^{-\kappa_j(\tilde{\mathbf{z}})} e^{ik_j}$  (of which Eq. 4 is a special case), we obtain  $D$  relations [121]  $\mathcal{F}_j(\tilde{\mathbf{z}}; k_j) = 0$ . Inverting these relations, we will in principle obtain  $D$  expressions  $z_j = \mathcal{F}_j(\mathbf{k})$  where  $\mathbf{k} \in \mathbb{T}^D$ , which generalize Eqs. 5a, 5b. In general, this nonlinear inversion may have to be performed numerically, and yields a highly complicated  $D$ -dimensional base manifold  $\mathcal{M}$  in  $\mathbf{z}$ -space, possibly with cusps and singularities that give rise to higher dimensional versions of esoteric gapped transitions [115]. The effective dimensional-transmuted BZ depends crucially on the topology of  $\mathcal{M}$ . Specifically, it is given by  $\mathcal{M}/\{\mathcal{L}\}$ , where  $\{\mathcal{L}\}$  is the span of homotopy loops  $l$  on  $\mathcal{M}$  in which  $E(\mathbf{z}(l))$  exhibits nontrivial spectral winding. In other words [121], the effective BZ is union of submanifolds of  $\mathbb{T}^D$  parametrized by  $(k'_1, \dots, k'_d), d < D$ , such that the recovered OBC spectrum  $\bar{E}(\mathbf{k}') = E(\mathbf{z}(\mathbf{k}'))$  exhibits trivial spectral winding in all directions (Eq. 6 gives a special case). As schematically sketched in Fig. 3d for a 3D model, the effective BZ consists of the blue and black loops which wind around  $\mathcal{M}$  (gray), not the red loop which encloses nonzero area on the spectral plane.

*Dimensional transmuted topology.*— The fundamental dimensional modification of the effective BZ by non-Hermitian pumping is not just a mathematical subtlety, but a very physical phenomenon with experimentally observable consequences. In the following, we illustrate a 2D lattice whose topological zero modes are protected by a 1D, not 2D, topological invariant due to dimensional transmutation of its BZ. Building upon our previous  $H_{2\text{D}}$

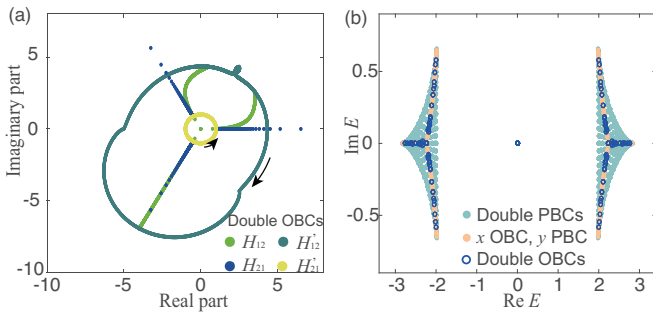


FIG. 4. a) Despite being a 2D model,  $H_{\text{topo}}$  exhibits nontrivial topological winding in its effectively 1D BZ, as seen from the zero windings of  $H_{12}(k)$  and  $H'_{12}(k')$  summing to  $-1$ , and that of  $H_{21}(k)$  and  $H'_{21}(k')$  summing to  $1$ . b) Although protected by 1D topological winding, in-gap zero modes for  $H_{\text{topo}}$  appear under double OBCs (black), and not quasi-1D single OBC (light blue). Parameters are  $t_1 = t_2 = t_3 = 1$  and  $c = 5$ .

example (Eq. 3), we consider the 2-component 2D model

$$H_{\text{topo}}(z) = \begin{pmatrix} 0 & z_x^\alpha + z_x^{-\beta} + z_x^{-\beta} z_y^{-a-b} + c z_y^{-a} \\ z_y^a & 0 \end{pmatrix}, \quad (7)$$

with constant  $c$  introduced such that the PBC spectrum  $E_{\text{topo}}(e^{ik_x}, e^{ik_y}) = \pm \sqrt{E_{2D}(e^{ik_x}, e^{ik_y}) + c}$  is gapped.

When regarded as a 2D model,  $H_{\text{topo}}$  is topologically trivial by construction, as can be seen from its Pauli decomposition  $H_{\text{topo}} = [(H_{12} + iH_{21})\sigma_x + (H_{12} - iH_{21})\sigma_y]/2$ , which contains only two Pauli matrices and is thus of trivial 2nd homotopy. However, the effective bulk description of  $H_{\text{topo}}$  is actually 1D, not 2D, since  $E_{\text{topo}}(z_x, z_y)$  and  $E_{2D}(z_x, z_y)$  are conformally related and must therefore possess identical effective 1D BZs [106, 108]. Under OBCs, an effectively 1D Hamiltonian possesses topological zero modes if the phase windings of  $H_{12}(z)$  and  $H_{21}(z)$  around  $z = 0$  are both nonzero and of opposite signs [84, 85]; if there is more than one BZ sector, the windings should be added [121]. This is indeed the case in Fig. 4a, with the windings of  $H_{12}$  and  $H'_{12}$  summing to  $-1$ , and that of  $H_{21}$  and  $H'_{21}$  summing to  $1$ . Correspondingly, these windings protect the isolated zero modes in the double OBCs spectrum (black diamond in Fig. 4b); these modes are topological since they appear in the double PBCs bandgap. Saliiently, despite being protected by 1D topological winding, they do not appear in the quasi-1D scenario of having  $x$ -OBCs alone (light blue).

*Discussion.*— Existing higher-dimensional non-Hermitian studies i.e. Chern or higher-order skin-topological characterizations [48, 80, 81, 116, 122, 123] have mostly been based on simple hyperlattices. Beyond that, in generic lattices with “entangled” couplings, we discover that non-Hermitian pumping does not commute, transmuting the momentum-space lattice (BZ) to an effectively lower dimension. This geometrical obstruction is rooted in a nonlinear inversion problem that is visualized as an incompletely “squashed” base BZ manifold. The classification

of how the lower-dimensional effective BZ winds around it gives rise to a novel instance of topological winding. As a fundamentally dynamical phenomenon, this dimensional transmutation contrasts with the dimensional reduction in topological classification [23, 78, 124], as well as the emergence of an extra scaling dimension in lattice-based holography approaches [125–128].

Physically, the dimensional transmutation can be manifested through bulk response and topological properties. Topological states protected by lower-dimensional invariants can be constructed and observed in open non-reciprocal arrays with sufficiently versatile engineered couplings, such as lossy photonic resonator arrays [34, 59, 129, 130], electrical circuits [34, 63, 64, 67, 68, 121, 131–143] or even quantum computers [144–148]. Additionally, quantum setups with well-defined state occupancy offer the tantalizing prospect for observing transport properties with altered dimensionality.

*Acknowledgements.*— This work is supported by MOE Tier 1 grant iRIMS no. 21-0048-P0001.

\* phyhuj@nus.edu.sg

† phylch@nus.edu.sg

- [1] David Bailin and Alex Love, “Kaluza-klein theories,” Reports on Progress in Physics **50**, 1087 (1987).
- [2] Juan Maldacena, “The large- $n$  limit of superconformal field theories and supergravity,” International journal of theoretical physics **38**, 1113–1133 (1999).
- [3] Edward Witten, “Anti de sitter space and holography,” arXiv preprint hep-th/9802150 (1998), 10.48550/arXiv.hep-th/9802150.
- [4] Steven S Gubser, Igor R Klebanov, and Alexander M Polyakov, “Gauge theory correlators from non-critical string theory,” Physics Letters B **428**, 105–114 (1998).
- [5] Pasquale Calabrese and John Cardy, “Entanglement entropy and conformal field theory,” Journal of physics a: mathematical and theoretical **42**, 504005 (2009).
- [6] John Cardy, “Conformal invariance and percolation,” arXiv preprint math-ph/0103018 (2001).
- [7] Michel Bauer and Denis Bernard, “Sle  $\kappa$  growth processes and conformal field theories,” Physics Letters B **543**, 135–138 (2002).
- [8] Guifre Vidal, José Ignacio Latorre, Enrique Rico, and Alexei Kitaev, “Entanglement in quantum critical phenomena,” Phys. Rev. Lett. **90**, 227902 (2003).
- [9] José Ignacio Latorre, Enrique Rico, and Guifré Vidal, “Ground state entanglement in quantum spin chains,” arXiv preprint quant-ph/0304098 (2003), 10.48550/arXiv.quant-ph/0304098.
- [10] Alexander R Its, Bai-Qi Jin, and Vladimir E Korepin, “Entanglement in the xy spin chain,” Journal of Physics A: Mathematical and General **38**, 2975 (2005).
- [11] Jacob JH Simmons, Peter Kleban, and Robert M Ziff, “Percolation crossing formulae and conformal field theory,” Journal of Physics A: Mathematical and Theoretical **40**, F771 (2007).
- [12] Sergey N Solodukhin, “Entanglement entropy, conformal invariance and extrinsic geometry,” Physics Letters

- B **665**, 305–309 (2008).
- [13] John Cardy and Pasquale Calabrese, “Unusual corrections to scaling in entanglement entropy,” *Journal of Statistical Mechanics: Theory and Experiment* **2010**, P04023 (2010).
- [14] Abbas Ali Saberi, “Recent advances in percolation theory and its applications,” *Physics Reports* **578**, 1–32 (2015).
- [15] Michael P Marder, *Condensed matter physics* (John Wiley & Sons, 2010).
- [16] Patrick A Lee and Daniel S Fisher, “Anderson localization in two dimensions,” *Phys. Rev. Lett.* **47**, 882 (1981).
- [17] M. Ya. Azbel, “Anderson-localization dimensionality dependence: Further comments,” *Phys. Rev. B* **26**, 4735–4738 (1982).
- [18] Aurélien Lherbier, Blanca Biel, Yann-Michel Niquet, and Stephan Roche, “Transport length scales in disordered graphene-based materials: Strong localization regimes and dimensionality effects,” *Phys. Rev. Lett.* **100**, 036803 (2008).
- [19] Amnon Aharony, Yoseph Imry, and Shang-keng Ma, “Lowering of dimensionality in phase transitions with random fields,” *Phys. Rev. Lett.* **37**, 1364 (1976).
- [20] A.D. Alekhin, “Critical indices for systems of different space dimensionality,” *Journal of Molecular Liquids* **120**, 43–45 (2005), *physics of Liquid Matter: Modern Problems*.
- [21] Alexander Altland and Martin R. Zirnbauer, “Non-standard symmetry classes in mesoscopic normal-superconducting hybrid structures,” *Phys. Rev. B* **55**, 1142–1161 (1997).
- [22] Andreas P. Schnyder, Shinsei Ryu, Akira Furusaki, and Andreas W. W. Ludwig, “Classification of topological insulators and superconductors in three spatial dimensions,” *Phys. Rev. B* **78**, 195125 (2008).
- [23] Shinsei Ryu, Andreas P Schnyder, Akira Furusaki, and Andreas WW Ludwig, “Topological insulators and superconductors: tenfold way and dimensional hierarchy,” *New Journal of Physics* **12**, 065010 (2010).
- [24] Alexei Kitaev, “Periodic table for topological insulators and superconductors,” in *AIP conference proceedings*, Vol. 1134 (American Institute of Physics, 2009) pp. 22–30.
- [25] Michael Stone, Ching-Kai Chiu, and Abhishek Roy, “Symmetries, dimensions and topological insulators: the mechanism behind the face of the bott clock,” *Journal of Physics A: Mathematical and Theoretical* **44**, 045001 (2010).
- [26] Takahiro Morimoto and Akira Furusaki, “Topological classification with additional symmetries from clifford algebras,” *Phys. Rev. B* **88**, 125129 (2013).
- [27] Ching-Kai Chiu, Hong Yao, and Shinsei Ryu, “Classification of topological insulators and superconductors in the presence of reflection symmetry,” *Phys. Rev. B* **88**, 075142 (2013).
- [28] Zongping Gong, Yuto Ashida, Kohei Kawabata, Kazuaki Takasan, Sho Higashikawa, and Masahito Ueda, “Topological phases of non-hermitian systems,” *Phys. Rev. X* **8**, 031079 (2018).
- [29] Chun-Hui Liu, Hui Jiang, and Shu Chen, “Topological classification of non-hermitian systems with reflection symmetry,” *Phys. Rev. B* **99**, 125103 (2019).
- [30] Linhu Li, Ching Hua Lee, and Jiangbin Gong, “Geometric characterization of non-hermitian topological systems through the singularity ring in pseudospin vector space,” *Phys. Rev. B* **100**, 075403 (2019).
- [31] Kohei Kawabata, Ken Shiozaki, Masahito Ueda, and Masatoshi Sato, “Symmetry and topology in non-hermitian physics,” *Phys. Rev. X* **9**, 041015 (2019).
- [32] Hengyun Zhou and Jong Yeon Lee, “Periodic table for topological bands with non-hermitian symmetries,” *Phys. Rev. B* **99**, 235112 (2019).
- [33] Zhi Li and Roger SK Mong, “Homotopical characterization of non-hermitian band structures,” *Phys. Rev. B* **103**, 155129 (2021).
- [34] Emil J Bergholtz, Jan Carl Budich, and Flore K Kunst, “Exceptional topology of non-hermitian systems,” *Reviews of Modern Physics* **93**, 015005 (2021).
- [35] Yi Chen Hu and Taylor L Hughes, “Absence of topological insulator phases in non-hermitian p t-symmetric hamiltonians,” *Phys. Rev. B* **84**, 153101 (2011).
- [36] Kenta Esaki, Masatoshi Sato, Kazuki Hasebe, and Mahito Kohmoto, “Edge states and topological phases in non-hermitian systems,” *Phys. Rev. B* **84**, 205128 (2011).
- [37] Tony E. Lee and Ching-Kit Chan, “Heralded magnetism in non-hermitian atomic systems,” *Phys. Rev. X* **4**, 041001 (2014).
- [38] Tony E Lee, Florentin Reiter, and Nimrod Moiseyev, “Entanglement and spin squeezing in non-hermitian phase transitions,” *Phys. Rev. Lett.* **113**, 250401 (2014).
- [39] Daniel Leykam, Konstantin Y. Bliokh, Chunli Huang, Y. D. Chong, and Franco Nori, “Edge modes, degeneracies, and topological numbers in non-hermitian systems,” *Phys. Rev. Lett.* **118**, 040401 (2017).
- [40] Wenchao Hu, Hailong Wang, Perry Ping Shum, and Y. D. Chong, “Exceptional points in a non-hermitian topological pump,” *Phys. Rev. B* **95**, 184306 (2017).
- [41] Simon Lieu, “Topological phases in the non-hermitian su-schrieffer-heeger model,” *Phys. Rev. B* **97**, 045106 (2018).
- [42] Chuanhao Yin, Hui Jiang, Linhu Li, Rong Lü, and Shu Chen, “Geometrical meaning of winding number and its characterization of topological phases in one-dimensional chiral non-hermitian systems,” *Phys. Rev. A* **97**, 052115 (2018).
- [43] Hui Jiang, Chao Yang, and Shu Chen, “Topological invariants and phase diagrams for one-dimensional two-band non-hermitian systems without chiral symmetry,” *Phys. Rev. A* **98**, 052116 (2018).
- [44] C. Li, X. Z. Zhang, G. Zhang, and Z. Song, “Topological phases in a kitaev chain with imbalanced pairing,” *Phys. Rev. B* **97**, 115436 (2018).
- [45] Huitao Shen, Bo Zhen, and Liang Fu, “Topological band theory for non-hermitian hamiltonians,” *Phys. Rev. Lett.* **120**, 146402 (2018).
- [46] Dan S. Borgnia, Alex Jura Kruchkov, and Robert-Jan Slager, “Non-hermitian boundary modes and topology,” *Phys. Rev. Lett.* **124**, 056802 (2020).
- [47] Lei Pan, Xin Chen, Yu Chen, and Hui Zhai, “Non-hermitian linear response theory,” *Nature Physics* **16**, 767–771 (2020).
- [48] Shunyu Yao, Fei Song, and Zhong Wang, “Non-hermitian chern bands,” *Phys. Rev. Lett.* **121**, 136802 (2018).
- [49] Jan Carl Budich, Johan Carlström, Flore K. Kunst, and Emil J. Bergholtz, “Symmetry-protected nodal phases

- in non-hermitian systems,” *Phys. Rev. B* **99**, 041406 (2019).
- [50] Ching Hua Lee, “Many-body topological and skin states without open boundaries,” *Phys. Rev. B* **104**, 195102 (2021).
- [51] Ruizhe Shen and Ching Hua Lee, “Non-hermitian skin clusters from strong interactions,” arXiv preprint arXiv:2107.03414 (2021).
- [52] Kohei Kawabata and Shinsei Ryu, “Nonunitary scaling theory of non-hermitian localization,” *Phys. Rev. Lett.* **126**, 166801 (2021).
- [53] Ching Hua Lee, “Exceptional bound states and negative entanglement entropy,” *Phys. Rev. Lett.* **128**, 010402 (2022).
- [54] Fang Qin, Ruizhe Shen, and Ching Hua Lee, “Non-hermitian squeezed polarons,” arXiv preprint arXiv:2202.10481 (2022).
- [55] Tiejun Gao, E Estrecho, KY Bliokh, TCH Liew, MD Fraser, Sebastian Brodbeck, Martin Kamp, Christian Schneider, Sven Höfling, Y Yamamoto, *et al.*, “Observation of non-hermitian degeneracies in a chaotic exciton-polariton billiard,” *Nature* **526**, 554–558 (2015).
- [56] Julia M. Zeuner, Mikael C. Rechtsman, Yonatan Plotnik, Yaakov Lumer, Stefan Nolte, Mark S. Rudner, Mordechai Segev, and Alexander Szameit, “Observation of a topological transition in the bulk of a non-hermitian system,” *Phys. Rev. Lett.* **115**, 040402 (2015).
- [57] Haitan Xu, David Mason, Luyao Jiang, and JGE Harris, “Topological energy transfer in an optomechanical system with exceptional points,” *Nature* **537**, 80 (2016).
- [58] L Xiao, X Zhan, ZH Bian, KK Wang, X Zhang, XP Wang, J Li, K Mochizuki, D Kim, N Kawakami, *et al.*, “Observation of topological edge states in parity-time-symmetric quantum walks,” *Nature Physics* **13**, 1117–1123 (2017).
- [59] Liang Feng, Ramy El-Ganainy, and Li Ge, “Non-hermitian photonics based on parity-time symmetry,” *Nature Photonics* **11**, 752 (2017).
- [60] Steffen Weimann, Manuel Kremer, Yonatan Plotnik, Yaakov Lumer, Stefan Nolte, Konstantinos G Makris, Mordechai Segev, Mikael C Rechtsman, and Alexander Szameit, “Topologically protected bound states in photonic parity-time-symmetric crystals,” *Nature materials* **16**, 433–438 (2017).
- [61] Midya Parto, Steffen Wittek, Hossein Hodaei, Gal Harari, Miguel A Bandres, Jinhan Ren, Mikael C Rechtsman, Mordechai Segev, Demetrios N Christodoulides, and Mercedeh Khajavikhan, “Edge-mode lasing in 1d topological active arrays,” *Phys. Rev. Lett.* **120**, 113901 (2018).
- [62] Sebastian Weidemann, Mark Kremer, Tobias Helbig, Tobias Hofmann, Alexander Stegmaier, Martin Greiter, Ronny Thomale, and Alexander Szameit, “Topological funneling of light,” *Science* **368**, 311–314 (2020).
- [63] T Helbig, T Hofmann, S Imhof, M Abdelghany, T Kiessling, LW Molenkamp, CH Lee, A Szameit, M Greiter, and R Thomale, “Generalized bulk-boundary correspondence in non-hermitian topoelectrical circuits,” *Nature Physics* , 1–4 (2020).
- [64] Tobias Hofmann, Tobias Helbig, Frank Schindler, Nora Salgo, Marta Brzezińska, Martin Greiter, Tobias Kiessling, David Wolf, Achim Vollhardt, Anton Kabaši, *et al.*, “Reciprocal skin effect and its realization in a topoelectrical circuit,” *Physical Review Research* **2**, 023265 (2020).
- [65] Lei Xiao, Tianshu Deng, Kunkun Wang, Gaoyan Zhu, Zhong Wang, Wei Yi, and Peng Xue, “Non-hermitian bulk-boundary correspondence in quantum dynamics,” *Nature Physics* **16**, 761–766 (2020).
- [66] Ananya Ghatak, Martin Brandenbourger, Jasper Van Wezel, and Corentin Coullais, “Observation of non-hermitian topology and its bulk-edge correspondence in an active mechanical metamaterial,” *Proceedings of the National Academy of Sciences* **117**, 29561–29568 (2020).
- [67] Deyuan Zou, Tian Chen, Wenjing He, Jiacheng Bao, Ching Hua Lee, Houjun Sun, and Xiangdong Zhang, “Observation of hybrid higher-order skin-topological effect in non-hermitian topoelectrical circuits,” *Nature Communications* **12**, 1–11 (2021).
- [68] Alexander Stegmaier, Stefan Imhof, Tobias Helbig, Tobias Hofmann, Ching Hua Lee, Mark Kremer, Alexander Fritzsche, Thorsten Feichtner, Sebastian Klemmt, Sven Höfling, *et al.*, “Topological defect engineering and p t symmetry in non-hermitian electrical circuits,” *Phys. Rev. Lett.* **126**, 215302 (2021).
- [69] Kai Wang, Avik Dutt, Charles C Wojcik, and Shan-hui Fan, “Topological complex-energy braiding of non-hermitian bands,” *Nature* **598**, 59–64 (2021).
- [70] He Gao, Haoran Xue, Zhongming Gu, Tuo Liu, Jie Zhu, and Baile Zhang, “Non-hermitian route to higher-order topology in an acoustic crystal,” *Nature communications* **12**, 1–7 (2021).
- [71] Weixuan Zhang, Fengxiao Di, Hao Yuan, Haiteng Wang, Xingen Zheng, Lu He, Houjun Sun, and Xiangdong Zhang, “Observation of non-hermitian many-body skin effects in hilbert space,” arXiv preprint arXiv:2109.08334 (2021).
- [72] Ce Shang, Shuo Liu, Ruiwen Shao, Peng Han, Xiaoning Zang, Xiangliang Zhang, Khaled Nabil Salama, Wenlong Gao, Ching Hua Lee, Ronny Thomale, *et al.*, “Experimental identification of the second-order non-hermitian skin effect with physics-graph-informed machine learning,” arXiv preprint arXiv:2203.00484 (2022).
- [73] Sebastian Weidemann, Mark Kremer, Stefano Longhi, and Alexander Szameit, “Topological triple phase transition in non-hermitian floquet quasicrystals,” *Nature* **601**, 354–359 (2022).
- [74] Haowei Li, Xiaoling Cui, and Wei Yi, “Non-hermitian skin effect in a spin-orbit-coupled bose-einstein condensate,” arXiv preprint arXiv:2201.01580 (2022).
- [75] Rodrigo Rosa-Medina, Francesco Ferri, Fabian Finger, Nishant Dogra, Katrin Kroeger, Rui Lin, R Chitra, Tobias Donner, and Tilman Esslinger, “Observing dynamical currents in a non-hermitian momentum lattice,” *Phys. Rev. Lett.* **128**, 143602 (2022).
- [76] D. J. Thouless, M. Kohmoto, M. P. Nightingale, and M. den Nijs, “Quantized hall conductance in a two-dimensional periodic potential,” *Phys. Rev. Lett.* **49**, 405–408 (1982).
- [77] Mahito Kohmoto, “Topological invariant and the quantization of the hall conductance,” *Annals of Physics* **160**, 343–354 (1985).
- [78] Xiao-Liang Qi, Taylor L Hughes, and Shou-Cheng Zhang, “Topological field theory of time-reversal invariant insulators,” *Phys. Rev. B* **78**, 195424 (2008).
- [79] Frank Schindler, Ashley M Cook, Maia G Vergniory,

- Zhijun Wang, Stuart SP Parkin, B Andrei Bernevig, and Titus Neupert, “Higher-order topological insulators,” *Science advances* **4**, eaat0346 (2018).
- [80] Ching Hua Lee, Linhu Li, and Jiangbin Gong, “Hybrid higher-order skin-topological modes in nonreciprocal systems,” *Phys. Rev. Lett.* **123**, 016805 (2019).
- [81] Xi-Wang Luo and Chuanwei Zhang, “Higher-order topological corner states induced by gain and loss,” *Phys. Rev. Lett.* **123**, 073601 (2019).
- [82] Hui Jiang and Ching Hua Lee, “Filling up complex spectral regions through non-hermitian disordered chains,” *Chinese Physics B* **31**, 050307 (2022).
- [83] This may not be the case for hyperbolic lattices [149–151], which can be realized in circuit setups [140, 152, 153].
- [84] Shunyu Yao and Zhong Wang, “Edge states and topological invariants of non-hermitian systems,” *Phys. Rev. Lett.* **121**, 086803 (2018).
- [85] Ching Hua Lee and Ronny Thomale, “Anatomy of skin modes and topology in non-hermitian systems,” *Phys. Rev. B* **99**, 201103 (2019).
- [86] Fei Song, Shunyu Yao, and Zhong Wang, “Non-hermitian topological invariants in real space,” *Phys. Rev. Lett.* **123**, 246801 (2019).
- [87] Fei Song, Shunyu Yao, and Zhong Wang, “Non-hermitian skin effect and chiral damping in open quantum systems,” *Phys. Rev. Lett.* **123**, 170401 (2019).
- [88] Stefano Longhi, “Probing non-hermitian skin effect and non-bloch phase transitions,” *Physical Review Research* **1**, 023013 (2019).
- [89] Kai Zhang, Zhesen Yang, and Chen Fang, “Correspondence between winding numbers and skin modes in non-hermitian systems,” *Phys. Rev. Lett.* **125**, 126402 (2020).
- [90] Kazuki Yokomizo and Shuichi Murakami, “Non-bloch band theory of non-hermitian systems,” *Phys. Rev. Lett.* **123**, 066404 (2019).
- [91] Zhesen Yang, Kai Zhang, Chen Fang, and Jiangping Hu, “Non-hermitian bulk-boundary correspondence and auxiliary generalized brillouin zone theory,” *Phys. Rev. Lett.* **125**, 226402 (2020).
- [92] Ching Hua Lee and Stefano Longhi, “Ultrafast and anharmonic rabi oscillations between non-bloch bands,” *Communications Physics* **3**, 1–9 (2020).
- [93] Stefano Longhi, “Non-bloch-band collapse and chiral zener tunneling,” *Phys. Rev. Lett.* **124**, 066602 (2020).
- [94] Jahan Claes and Taylor L. Hughes, “Skin effect and winding number in disordered non-hermitian systems,” *Phys. Rev. B* **103**, L140201 (2021).
- [95] Nobuyuki Okuma, Kohei Kawabata, Ken Shiozaki, and Masatoshi Sato, “Topological origin of non-hermitian skin effects,” *Phys. Rev. Lett.* **124**, 086801 (2020).
- [96] Frank Schindler and Abhinav Prem, “Dislocation non-hermitian skin effect,” *Phys. Rev. B* **104**, L161106 (2021).
- [97] Linhu Li, Ching Hua Lee, and Jiangbin Gong, “Impurity induced scale-free localization,” *Communications Physics* **4**, 1–9 (2021).
- [98] Nobuyuki Okuma and Masatoshi Sato, “Non-hermitian skin effects in hermitian correlated or disordered systems: Quantities sensitive or insensitive to boundary effects and pseudo-quantum-number,” *Phys. Rev. Lett.* **126**, 176601 (2021).
- [99] Linhu Li, Sen Mu, Ching Hua Lee, and Jiangbin Gong, “Quantized classical response from spectral winding topology,” *Nature communications* **12**, 1–11 (2021).
- [100] Cui-Xian Guo, Chun-Hui Liu, Xiao-Ming Zhao, Yanxia Liu, and Shu Chen, “Exact solution of non-hermitian systems with generalized boundary conditions: Size-dependent boundary effect and fragility of the skin effect,” *Phys. Rev. Lett.* **127**, 116801 (2021).
- [101] Linhu Li and Ching Hua Lee, “Non-hermitian pseudogaps,” *Science Bulletin* **67**, 685–690 (2022).
- [102] Russell Yang, Jun Wei Tan, Tommy Tai, Jin Ming Koh, Linhu Li, Stefano Longhi, and Ching Hua Lee, “Designing non-hermitian real spectra through electrostatics,” *arXiv preprint arXiv:2201.04153* (2022).
- [103] SM Rafi-Ul-Islam, Zhuo Bin Siu, Haydar Sahin, Ching Hua Lee, and Mansoor Jalil, “System size dependent topological zero modes in coupled topoelectrical chains,” *arXiv preprint arXiv:2206.05298* (2022).
- [104] Wen-Tan Xue, Yu-Min Hu, Fei Song, and Zhong Wang, “Non-hermitian edge burst,” *Phys. Rev. Lett.* **128**, 120401 (2022).
- [105] Boxue Zhang, Qingya Li, Xiao Zhang, and Ching Hua Lee, “Real non-hermitian energy spectra without any symmetry,” *Chinese Physics B* **31**, 070308 (2022).
- [106] T. Tai and C. H. Lee, “Zoology of non-hermitian spectra and their graph topology,” *arXiv e-prints* (2022), 10.48550/arXiv.2202.03462.
- [107] Which arises even if all couplings are local.
- [108] Ching Hua Lee, Linhu Li, Ronny Thomale, and Jiangbin Gong, “Unraveling non-hermitian pumping: Emergent spectral singularities and anomalous responses,” *Phys. Rev. B* **102**, 085151 (2020).
- [109] M. V. Berry, “Quantal phase factors accompanying adiabatic changes,” *Proceedings of the Royal Society of London A: Mathematical, Physical and Engineering Sciences* **392**, 45–57 (1984).
- [110] Adrian Bachtold, Christoph Strunk, Jean-Paul Salvetat, Jean-Marc Bonard, Laszo Forro, Thomas Nussbaumer, and Christian Schonenberger, “Aharonov–bohm oscillations in carbon nanotubes,” *Nature* **397**, 673–675 (1999).
- [111] Wei Gou, Tao Chen, Dizhou Xie, Teng Xiao, Tian-Shu Deng, Bryce Gadway, Wei Yi, and Bo Yan, “Tunable non-reciprocal quantum transport through a dissipative aharonov-bohm ring in ultracold atoms,” *Phys. Rev. Lett.* **124**, 070402 (2020).
- [112] Naomichi Hatano and David R. Nelson, “Localization transitions in non-hermitian quantum mechanics,” *Phys. Rev. Lett.* **77**, 570–573 (1996).
- [113] Naomichi Hatano and David R. Nelson, “Vortex pinning and non-hermitian quantum mechanics,” *Phys. Rev. B* **56**, 8651–8673 (1997).
- [114] Stefano Longhi, Davide Gatti, and Giuseppe Della Valle, “Non-hermitian transparency and one-way transport in low-dimensional lattices by an imaginary gauge field,” *Phys. Rev. B* **92**, 094204 (2015).
- [115] Linhu Li, Ching Hua Lee, Sen Mu, and Jiangbin Gong, “Critical non-hermitian skin effect,” *Nature communications* **11**, 1–8 (2020).
- [116] Kohei Kawabata, Masatoshi Sato, and Ken Shiozaki, “Higher-order non-hermitian skin effect,” *Phys. Rev. B* **102**, 205118 (2020).
- [117] Chun-Hui Liu, Kai Zhang, Zhesen Yang, and Shu Chen, “Helical damping and dynamical critical skin effect in open quantum systems,” *Physical Review Research* **2**,

- 043167 (2020).
- [118] Kazuki Yokomizo and Shuichi Murakami, “Scaling rule for the critical non-hermitian skin effect,” *Phys. Rev. B* **104**, 165117 (2021).
- [119] Kohei Kawabata, Tokiro Numasawa, and Shinsei Ryu, “Entanglement phase transition induced by the non-hermitian skin effect,” arXiv preprint arXiv:2206.05384 (2022).
- [120] This can be seen via a complex flux threading Gedanken experiment [85, 99, 154]. Gauge transforming all flux  $\phi$  onto the boundary coupling, the latter shrinks when we ramp up  $\text{Im}(\phi)$ ; correspondingly, the effect of cycling  $\text{Re}(\phi)$  across  $[0, 2\pi]$  diminishes. In the OBC limit, further spectral flow is not possible, and only degenerate spectral loops can exist.
- [121] “Supplemental materials,” Supplemental Materials.
- [122] Motohiko Ezawa, “Electric-circuit realization of non-hermitian higher-order topological systems,” 1810.04527v1.
- [123] Solofo Groenendijk, Thomas L Schmidt, and Tobias Meng, “Universal hall conductance scaling in non-hermitian chern insulators,” *Physical Review Research* **3**, 023001 (2021).
- [124] Nathanan Tantisavasadakarn, “Dimensional reduction and topological invariants of symmetry-protected topological phases,” *Phys. Rev. B* **96**, 195101 (2017).
- [125] Xiao-Liang Qi, “Exact holographic mapping and emergent space-time geometry,” arXiv preprint arXiv:1309.6282 (2013).
- [126] Yingfei Gu, Ching Hua Lee, Xueda Wen, Gil Young Cho, Shinsei Ryu, and Xiao-Liang Qi, “Holographic duality between (2+1)-dimensional quantum anomalous hall state and (3+1)-dimensional topological insulators,” *Phys. Rev. B* **94**, 125107 (2016).
- [127] Ching Hua Lee, “Generalized exact holographic mapping with wavelets,” *Phys. Rev. B* **96**, 245103 (2017).
- [128] Hong-Ye Hu, Shuo-Hui Li, Lei Wang, and Yi-Zhuang You, “Machine learning holographic mapping by neural network renormalization group,” *Physical Review Research* **2**, 023369 (2020).
- [129] LC Botten, RC McPhedran, NA Nicorovici, and GH Derrick, “Periodic models for thin optimal absorbers of electromagnetic radiation,” *Phys. Rev. B* **55**, R16072 (1997).
- [130] Amnon Yariv, “Critical coupling and its control in optical waveguide-ring resonator systems,” *IEEE Photonics Technology Letters* **14**, 483–485 (2002).
- [131] Ching Hua Lee, Stefan Imhof, Christian Berger, Florian Bayer, Johannes Brehm, Laurens W Molenkamp, Tobias Kiessling, and Ronny Thomale, “Topolectrical circuits,” *Communications Physics* **1**, 1–9 (2018).
- [132] Stefan Imhof, Christian Berger, Florian Bayer, Johannes Brehm, Laurens W Molenkamp, Tobias Kiessling, Frank Schindler, Ching Hua Lee, Martin Greiter, Titus Neupert, *et al.*, “Topolectrical-circuit realization of topological corner modes,” *Nature Physics* **14**, 925 (2018).
- [133] Tobias Helbig, Tobias Hofmann, Ching Hua Lee, Ronny Thomale, Stefan Imhof, Laurens W Molenkamp, and Tobias Kiessling, “Band structure engineering and reconstruction in electric circuit networks,” *Phys. Rev. B* **99**, 161114 (2019).
- [134] Tobias Hofmann, Tobias Helbig, Ching Hua Lee, Martin Greiter, and Ronny Thomale, “Chiral voltage propagation and calibration in a topolectrical chern circuit,” *Phys. Rev. Lett.* **122**, 247702 (2019).
- [135] Tejas Kotwal, Fischer Moseley, Alexander Stegmaier, Stefan Imhof, Hauke Brand, Tobias Kießling, Ronny Thomale, Henrik Ronellenfitsch, and Jörn Dunkel, “Active topolectrical circuits,” *Proceedings of the National Academy of Sciences* **118**, e2106411118 (2021).
- [136] Zhi-Qiang Zhang, Bing-Lan Wu, Juntao Song, and Hua Jiang, “Topological anderson insulator in electric circuits,” *Phys. Rev. B* **100**, 184202 (2019).
- [137] Xiang Ni, Zhicheng Xiao, Alexander B Khanikaev, and Andrea Alù, “Robust multiplexing with topolectrical higher-order chern insulators,” *Phys. Rev. Applied* **13**, 064031 (2020).
- [138] Ching Hua Lee, Amanda Sutrisno, Tobias Hofmann, Tobias Helbig, Yuhan Liu, Yee Sin Ang, Lay Kee Ang, Xiao Zhang, Martin Greiter, and Ronny Thomale, “Imaging nodal knots in momentum space through topolectrical circuits,” *Nature communications* **11**, 1–13 (2020).
- [139] Xiao-Xiao Zhang and Marcel Franz, “Non-hermitian exceptional landau quantization in electric circuits,” *Phys. Rev. Lett.* **124**, 046401 (2020).
- [140] Patrick M Lenggenhager, Alexander Stegmaier, Lavi K Upreti, Tobias Hofmann, Tobias Helbig, Achim Vollhardt, Martin Greiter, Ching Hua Lee, Stefan Imhof, Hauke Brand, *et al.*, “Electric-circuit realization of a hyperbolic drum,” arXiv preprint arXiv:2109.01148 (2021).
- [141] Shuo Liu, Ruiwen Shao, Shaojie Ma, Lei Zhang, Oubo You, Haotian Wu, Tie Cui, and Shuang Zhang, “Non-hermitian skin effect in a non-hermitian electrical circuit,” *Research* **2021**, 1–9 (2021).
- [142] Shuo Liu, Shaojie Ma, Cheng Yang, Lei Zhang, Wenlong Gao, Yuan Jiang Xiang, Tie Jun Cui, and Shuang Zhang, “Gain- and loss-induced topological insulating phase in a non-hermitian electrical circuit,” *Phys. Rev. Applied* **13**, 014047 (2020).
- [143] Hendrik Hohmann, Tobias Hofmann, Tobias Helbig, Stefan Imhof, Hauke Brand, Lavi K Upreti, Alexander Stegmaier, Alexander Fritzsche, Tobias Müller, Udo Schwingenschlögl, *et al.*, “Observation of cnoidal wave localization in non-linear topolectric circuits,” arXiv preprint arXiv:2206.09931 (2022).
- [144] Kenny Choo, Curt W Von Keyserlingk, Nicolas Regnault, and Titus Neupert, “Measurement of the entanglement spectrum of a symmetry-protected topological state using the ibm quantum computer,” *Phys. Rev. Lett.* **121**, 086808 (2018).
- [145] Adam Smith, MS Kim, Frank Pollmann, and Johannes Knolle, “Simulating quantum many-body dynamics on a current digital quantum computer,” *npj Quantum Information* **5**, 1–13 (2019).
- [146] Bikash K Behera, Tasnum Reza, Angad Gupta, and Prasanta K Panigrahi, “Designing quantum router in ibm quantum computer,” *Quantum Information Processing* **18**, 1–13 (2019).
- [147] Daniel Azzes, Rafael Haenel, Yehuda Naveh, Robert Raussendorf, Eran Sela, and Emanuele G Dalla Torre, “Identification of symmetry-protected topological states on noisy quantum computers,” *Phys. Rev. Lett.* **125**, 120502 (2020).
- [148] Jin Ming Koh, Tommy Tai, Yong Han Phee, Wei En Ng, and Ching Hua Lee, “Stabilizing multiple topolog-

- ical fermions on a quantum computer,” *npj Quantum Information* **8**, 1–10 (2022).
- [149] Joseph Maciejko and Steven Rayan, “Hyperbolic band theory,” *Science advances* **7**, eabe9170 (2021).
- [150] Joseph Maciejko and Steven Rayan, “Automorphic bloch theorems for hyperbolic lattices,” *Proceedings of the National Academy of Sciences* **119**, e2116869119 (2022).
- [151] Igor Boettcher, Alexey V Gorshkov, Alicia J Kollár, Joseph Maciejko, Steven Rayan, and Ronny Thomale, “Crystallography of hyperbolic lattices,” *Phys. Rev. B* **105**, 125118 (2022).
- [152] Alicia J Kollár, Mattias Fitzpatrick, and Andrew A Houck, “Hyperbolic lattices in circuit quantum electrodynamics,” *Nature* **571**, 45–50 (2019).
- [153] Igor Boettcher, Przemyslaw Bienias, Ron Belyansky, Alicia J Kollár, and Alexey V Gorshkov, “Quantum simulation of hyperbolic space with circuit quantum electrodynamics: From graphs to geometry,” *Phys. Rev. A* **102**, 032208 (2020).
- [154] Ye Xiong, “Why does bulk boundary correspondence fail in some non-hermitian topological models,” *Journal of Physics Communications* **2**, 035043 (2018).
- [155] Andrea Crespi, Giacomo Corrielli, Giuseppe Della Valle, Roberto Osellame, and Stefano Longhi, “Dynamic band collapse in photonic graphene,” *New Journal of Physics* **15**, 013012 (2013).
- [156] Jia Ningyuan, Clai Owens, Ariel Sommer, David Schuster, and Jonathan Simon, “Time-and site-resolved dynamics in a topological circuit,” *Phys. Rev. X* **5**, 021031 (2015).
- [157] Motohiko Ezawa, “Non-hermitian higher-order topological states in nonreciprocal and reciprocal systems with their electric-circuit realization,” *Phys. Rev. B* **99**, 201411 (2019).
- [158] Xiao Zhang, Boxue Zhang, Haydar Sahin, Zhuo Bin Siu, SM Rafi-Ul-Islam, Jian Feng Kong, Mansoor Jalil, Ronny Thomale, and Ching Hua Lee, “Anomalous fractal scaling in two-dimensional electric networks,” *arXiv preprint arXiv:2204.05329* (2022).

## Supplementary Materials

### ANALYTIC GBZ RESULTS FOR GENERIC 1D SYSTEMS WITH TWO TERMS

As a foundation for the analysis of the effective BZ of higher-dimensional lattices, we develop in this section a general analytic derivation for the generalized Brillouin zone (GBZ) results for 1D systems with 2 hopping terms, and compare them with numerics. In this supplement, we shall refer to “GBZ” and “effective BZ” interchangeably. Note that these results may no longer hold when there are more than 2 hopping terms, which is the more interesting scenario which this work is concerned with.

#### Preliminaries

Consider the following 1D single-band model with dissimilar left/right hoppings:

$$H_{1D} = \sum_n A|n\rangle\langle n + \alpha| + B|n\rangle\langle n - \beta| , \quad (S1)$$

whose eigenvalues are  $E(z) = Az^\alpha + Bz^{-\beta}$ , where  $z = e^{ik}$  describes the momentum component normal to the boundary of interest. This effective 1D single-band system has only 2 hoppings, one is to move  $\alpha$  sites to the left by amplitude  $A$ , the other with amplitude  $B$ ,  $\beta$  sites to the right. In higher-dimensional contexts,  $A$  and  $B$  can depend on the momenta from the other directions.

Corresponding to this eigenvalue  $E(z) = Az^\alpha + Bz^{-\beta}$  is the eigenstate  $|\psi(z)\rangle$ . In deference to Bloch’s theorem, we assume that it takes the form of a *generalized* Bloch state given by the ansatz  $|\psi(z)\rangle = (\dots, \psi_n(z), \dots)^T$ ,  $\psi_n(z) = z^n$ , position index  $n$ , which satisfies the bulk equation

$$A\psi_{n+\alpha}(z) + B\psi_{n-\beta}(z) = E(z)\psi_n(z) . \quad (S2)$$

At a particular energy  $E(z)$ , there exists other wavefunction solutions  $|\psi(z')\rangle$  which satisfies the same eigenvalue  $E(z)$ , i.e.

$$Az'^\alpha + Bz'^{-\beta} - E(z) = 0 . \quad (S3)$$

This equation above is a polynomial relation of order  $\alpha + \beta$  in  $z$ , and it’s easy to get its solutions  $z_1, z_2, \dots, z_{\alpha+\beta}$ , which can all be expressed in terms of  $z$ . These solutions shall provide information about how  $z$  is controlled by hopping amplitudes  $A$  and  $B$ .

Hereupon, an eigensolution  $|\Psi\rangle$  with eigenenergy  $E(z)$  can be written as

$$|\Psi\rangle = \sum_{i=1}^{\alpha+\beta} c_i |\psi(z_i)\rangle , \quad (S4)$$

with coefficients  $c_i$  ( $i = 1, 2, \dots, \alpha + \beta$ ). To determine how they are constrained, we apply open boundary conditions onto  $|\Psi\rangle$ , arriving at

$$\Psi_{n'} = \sum_{i=1}^{\alpha+\beta} c_i z_i^{n'} = 0 , \quad n' = 0, -1, -2, \dots, 1 - \beta \quad \text{or} \quad L + 1, L + 2, \dots, L + \alpha , \quad (S5)$$

that is, there have  $\alpha + \beta$  constraints from the open boundary conditions (OBCs), which together combine to form the GBZ characteristic equation

$$\det M = \sum_{n_1, n_2, \dots, n_{\alpha+\beta}=1}^{\alpha+\beta} \varepsilon_{n_1, n_2, \dots, n_{\alpha+\beta}} z_{n_1}^{1-\beta} \times z_{n_2}^{2-\beta} \times \dots \times z_{n_\beta}^0 \times z_{n_{\beta+1}}^{L+1} \times z_{n_{\beta+2}}^{L+2} \times \dots \times z_{n_{\alpha+\beta}}^{L+\alpha} = 0 , \quad (S6)$$

where the matrix  $M$  is  $(\alpha + \beta) \times (\alpha + \beta)$  square array,  $\varepsilon_{n_1, n_2, \dots, n_{\alpha+\beta}}$  is  $\alpha + \beta$ -order arrangement, and  $\varepsilon_{n_1, n_2, \dots, n_{\alpha+\beta}} = -1$ , when  $n_1, n_2, \dots, n_{\alpha+\beta}$  is odd arrangement,  $\varepsilon_{n_1, n_2, \dots, n_{\alpha+\beta}} = 1$  if  $n_1, n_2, \dots, n_{\alpha+\beta}$  is even arrangement. Since

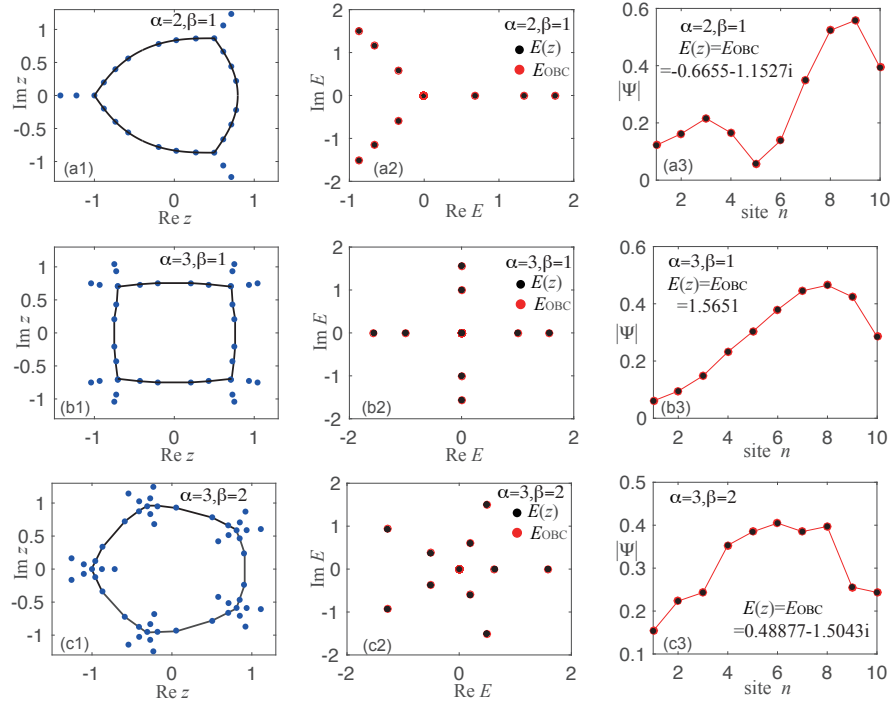


FIG. S1. (a1–c1) Solutions  $z$  to the characteristic equation (Eq.(S6)) for a few illustrative values of  $\alpha, \beta$ , with  $A = B = 1$  and system size of  $L = 10$  sites. Blue dots represent the full set of solutions, but only those lying on the black constraint curves constitute the actual GBZ solutions for OBCs. (a2–c2) Their corresponding eigenenergies  $E(z) = Az^\alpha + bz^{-\beta}$  (black) are the set of  $z$  points belonging to the GBZ, which agree excellently with  $E_{\text{OBC}}$  (red) of Eq.(S1). (a3–c3) shows the excellent agreement between numerical eigenstate solutions (red) and their corresponding GBZ solutions (black).

$z_1, z_2, \dots, z_{\alpha+\beta}$  are all functions of  $z$ , the GBZ characteristic equation Eq.(S6) is in actuality only a function of  $z$ .

Taking the model Eq.(S1) with  $\alpha = 2, \beta = 1$  as a sample, the eigenvalues  $E(z) = Az^2 + B/z$  can be obtained by bulk equation Eq.(S6). Considering the same eigenenergy  $E(z)$ , the eigensolution  $|\Psi\rangle = \sum_{i=1}^3 c_i |\psi(z_i)\rangle$ ,  $\psi_n(z_i) = z_i^n$ , and  $z_i$  which satisfy  $Az_i^2 + B/z_i - E(z) = 0$ , are constrained by  $z$  and hopping amplitude  $A, B$

$$z_1 = z, \quad z_2 = -\frac{z}{2} + \sqrt{\frac{B}{Az} + \frac{z^2}{4}}, \quad z_3 = -\frac{z}{2} - \sqrt{\frac{B}{Az} + \frac{z^2}{4}}. \quad (\text{S7})$$

Applying open boundary conditions into  $|\Psi\rangle$ , we can get GBZ characteristic equation

$$\det M = \det \begin{pmatrix} 1 & 1 & 1 \\ z_1^{L+1} & z_2^{L+1} & z_3^{L+1} \\ z_1^{L+2} & z_2^{L+2} & z_3^{L+2} \end{pmatrix} = (z_1 z_2)^{L+1} (z_2 - z_1) + (z_1 z_3)^{L+1} (z_1 - z_3) + (z_2 z_3)^{L+1} (z_3 - z_2) = 0, \quad (\text{S8})$$

which is only a function of  $z$ . The determinant must vanish so that we have a nontrivial eigenstate solution  $(c_1, c_2, c_3)^T$  of the matrix  $M$  with eigenvalue 0. It is worth noting that not all the solution  $z$  of GBZ characteristic equation Eq.(S8) is GBZ results of the system, as show in FIG. S1(a1–a3). To put it simply, for fixed  $z$ ,  $z_1, z_2, z_3$  which are from Eq.(S7) can be rearranged by  $|z_1| \leq |z_2| \leq |z_3|$ . If the absolute value  $|z_3|$  is not equal to  $|z_2|$ , we have  $\lim_{L \gg 1} c_3 = 0, (c_1 = -c_2)$ , that is, the solution  $z_3$  does not belong to GBZ. And in other cases, we can also select GBZ solutions from the set of solution  $z$  by the values of the coefficients  $c_1, c_2, c_3$ .

### Determination of the GBZ for OBCs

However, not all solutions  $z$  of the characteristic equation Eq.(S6) contribute to the actual OBC solutions. Those that do define the GBZ. In Figs. S1(a1–c1), we see that of all solutions  $z$  (blue dots), only those that lie on the black

curves correspond to values of  $E(z)$  that coincide with actual numerically obtained eigenvalues (Figs. S1(a2—c2)).

From known results on GBZ construction [85, 91, 108], solutions  $z$  that belong to the GBZ (i.e. black curves) are those  $z$  such that there exists another  $z' \neq z$  such that  $|z| = |z'|$  and  $E(z) = E(z')$ . If more than one such pair of solutions exist, the GBZ is defined by the pair with  $|z| = |z'|$  closest to unity. This is because  $|z|$  determines the spatial decay rate of the eigensolution, and the GBZ pair is given by the pair of solutions that are mostly slowly decaying, and yet able to satisfy OBCs at both boundaries (which can be arbitrarily far) simultaneously. In other words, the GBZ is obtained through the pair among  $z_1, z_2, \dots, z_{\alpha+\beta}$  with the same absolute value.

Let's now solve for the GBZ of our 1D lattice  $H_{1D}$ , with  $z$  parametrized by a wavenumber  $k$ . First, we write the two degenerate solutions of  $z$  as  $z_{\pm} = z_0 e^{ik' \pm k}$ , with real  $k', k$  and possessing the same energy  $E(z_{\pm})$ . Here  $z_0$  is a parameter that is unspecified for now. Taking  $z_{\pm}$  into the energy equation,

$$E = E(z_+) = E(z_-) = Az_0^{\alpha} e^{i\alpha(k'+k)} + Bz_0^{-\beta} e^{i\beta(k'+k)} = Az_0^{\alpha} e^{i\alpha(k'-k)} + Bz_0^{-\beta} e^{-i\beta(k'-k)}. \quad (\text{S9})$$

As such, we can solve for  $z_{\pm}$ :

$$z_{\pm} = \left( \frac{B \sin \beta k}{A \sin \alpha k} \right)^{\frac{1}{\alpha+\beta}} e^{\pm ik + i \frac{2\pi v}{\alpha+\beta}}, \quad (\text{S10})$$

with  $v = 1, 2, \dots, \alpha + \beta$ . Note that  $|z_{\pm}| \neq 1$  in general, and only when  $k = n\pi/(\alpha + \beta)$  do we have  $|\sin \beta k|/|\sin \alpha k| = 1$ . Due to the periodicity of  $2\pi/(\alpha + \beta)$ , without loss of generality, we shall from now on set the range of parameter  $k$  to be  $[n\pi - \pi/(\alpha + \beta), n\pi + \pi/(\alpha + \beta))$ , with integer  $n$ . For definiteness, we take  $n = 0$ .

In all, the GBZ of our model  $H_{1D}$  (Eq.(S1)) is given by

$$\text{GBZ}_{1D} = \left\{ z = \left( \frac{B \sin \beta k}{A \sin \alpha k} \right)^{\frac{1}{\alpha+\beta}} e^{ik + i \frac{2\pi v}{\alpha+\beta}} \mid k = \left( -\frac{\pi}{\alpha + \beta}, \frac{\pi}{\alpha + \beta} \right], v = 1, 2, \dots, \alpha + \beta \right\}, \quad (\text{S11})$$

which gives energies

$$\bar{E}(k) = E(z) = Az^{\alpha} + Bz^{-\beta} = \left( \frac{A^{\beta} B^{\alpha}}{(\sin(\alpha k))^{\alpha} (\sin(\beta k))^{\beta}} \right)^{\frac{1}{\alpha+\beta}} \sin((\alpha + \beta)k) e^{\frac{2i\pi\alpha v}{\alpha+\beta}}, \quad (\text{S12})$$

which agrees closely with numerical OBC eigenenergies in Figs. S1(a2—c2). Here, the bar above  $\bar{E}(k)$  indicates that the energy function is evaluated on the GBZ, i.e. it depends on  $k$  not on the ordinary BZ, but through the GBZ. Eq. S11 is a main result that will be used in the GBZ computation of higher-dimensional cases later on. As consistent with the fact that OBC spectra cannot undergo any further NHSE (in the same direction), the spectral winding of  $E(z)$  above is always zero, that is, the distribution of  $E(z)$  in the complex plane cannot form closed curves.

In generic 1D lattices with multiple hopping terms, Eq. S9 will have to be replaced by a simultaneously polynomial relations which has to be solved numerically. The resultant GBZ is still well-defined, although it is likely obtainable only numerically.

## 2D NON-HERMITIAN LATTICES WITH 2D GBZS

This section introduces how the GBZ can be obtained for 2D lattices through a few concrete examples with different hopping terms.

### 2D lattice model with 2 hopping terms

To connect with our previous treatment of 1D lattices with 2 hopping terms, we first consider the simplest case of 2D lattices with 2 hopping terms:

$$H_{2D,2} = \sum_{m,n} t|m,n\rangle\langle m + \alpha, n + a| + t'|m,n\rangle\langle m - \beta, n - b|, \quad (\text{S13})$$

with hoppings of amplitudes  $t$  (or  $t'$ ) corresponding to transitions of  $(-\alpha, -a)$  sites ( or  $(\beta, b)$  sites) on the lattice.

We consider the ansatz  $|\psi\rangle \propto \sum_{m,n} \psi_{mn} |m, n\rangle$  with  $\psi_{mn} = z_x^m z_y^n$ . In the bulk, it gives eigenenergies  $E(z_x, z_y)$

$$E(z_x, z_y) = tz_x^\alpha z_y^a + t' z_x^{-\beta} z_y^{-b}. \quad (\text{S14})$$

For a fixed  $z_x$ , there are  $a + b$  solutions  $z_{y,i}$ , ( $i = 1, 2, \dots, a + b$ ) corresponding to the same energy  $E(z_x, z_y)$ . Similarly, we can also find  $\alpha + \beta$  solutions  $z_{x,j}$ , ( $j = 1, 2, \dots, \alpha + \beta$ ) corresponding to fixed  $E(z_x, z_y)$  and  $z_y$ . Both sets of solutions  $z_{y,i}$ , ( $i = 1, 2, \dots, a + b$ ) and  $z_{x,j}$ , ( $j = 1, 2, \dots, \alpha + \beta$ ) can be written entirely in terms of  $z_x$  and  $z_y$ .

We next show a detailed derivation of the GBZ of  $H_{2D,2}$ . For a quick heuristic approach, the reader may directly skip to Eqs. S16 and S17.

Implementing open boundary conditions on the wavefunction  $|\Psi\rangle$  for a fixed eigenenergy  $E(z_x, z_y)$  gives

$$\begin{aligned} |\Psi\rangle = |\Psi^1\rangle = |\Psi^2\rangle &\propto \sum_{m,n} \Psi_{mn} |m, n\rangle = \sum_{m,n} \Psi_{mn}^1 |m, n\rangle = \sum_{m,n} \Psi_{mn}^2 |m, n\rangle, \\ \Psi_{mn}^1 &= \sum_{z_y} \left( \left( \sum_j^{\alpha+\beta} f_{z_x,j} z_{x,j}^m \right) g_{z_y} z_y^n \right), \quad \Psi_{mn}^2 = \sum_{z_x} \left( f_{z_x} z_x^m \left( \sum_i^{a+b} g_{z_y,i} z_{y,i}^n \right) \right), \end{aligned} \quad (\text{S15})$$

Here, we have written  $|\Psi\rangle$  either as  $|\Psi^1\rangle$  or  $|\Psi^2\rangle$ , depending on the order of expansion in terms of the  $x$  and  $y$  coefficients. These two ways to expand are of course equivalent, and note the relation  $f_{z_x} g_{z_y,i} = g_{z_y,i} f_{z_x}$ . The  $\sum_i, \sum_j$  summations in  $\Psi_{mn}^1, \Psi_{mn}^2$  refers to sums over all sets  $z_x, z_y$  which have same energy  $E$ . To treat boundary conditions along different direction (i.e.,  $\mathbf{x}, \mathbf{y}$  directions), we can choose the appropriate expansion and proceed like in the 1D case (see Sec. ), paying careful attention to the indices i.e. for OBCs along the  $\mathbf{x}$  direction, we have  $\Psi_{m'n} = \Psi_{m'n}^1 = 0$  for any  $n$  and  $m' = -\beta + 1, -\beta + 2, \dots, L + 1, L + 2, \dots, L + \alpha$  (assuming  $\alpha, \beta > 0$ ). Thus we obtain

$$z_x^{\alpha+\beta} = \frac{t'}{t} \frac{z_1^{\alpha+\beta}}{z_y^{a+b}}, \quad z_1^{\alpha+\beta} = \frac{\sin \beta k_1}{\sin \alpha k_1} e^{i(\alpha+\beta)k_1}, \quad (\text{S16})$$

with momentum parameter  $k_1 \in \left(-\frac{\pi}{\alpha+\beta}, \frac{\pi}{\alpha+\beta}\right]$  as in a quasi-1D case (see Sec. for details). Likewise, considering the expansion via  $|\Psi\rangle = |\Psi^2\rangle$  with boundary conditions along the  $\mathbf{y}$  direction, we obtain the alternative expressions

$$z_y^{a+b} = \frac{t'}{t} \frac{z_2^{a+b}}{z_x^{\alpha+\beta}}, \quad z_2^{a+b} = \frac{\sin b k_2}{\sin a k_2} e^{i(a+b)k_2}, \quad (\text{S17})$$

with  $k_2 \in \left(-\frac{\pi}{a+b}, \frac{\pi}{a+b}\right]$ . To solve for the GBZs of simultaneous x-OBCs and y-OBCs in 2D, we simultaneously solve Eqs. S16 and S17. Note that heuristically, Eqs. S16 and S17 can be simply written down by treating  $H_{2D,2}$  as a 1D chain with hoppings dependent on the transverse momentum. For instance, we can write Eq. S14 either as  $E(z_x) = (tz_y^a)z_x^\alpha + (tz_y^{-b})z_x^{-\beta}$  or  $E(z_y) = (tz_x^\alpha)z_y^a + (tz_x^{-\beta})z_y^{-b}$ , and apply Eq. S11 to obtain Eqs. S16 and S17 respectively. Importantly, we shall see that this approach fails in general 2D lattices, even though it is valid in this case where there are only two hopping terms from each site.

In the following, we shall specialize to the case where the two hoppings are pointing in the same direction i.e.  $\alpha/\beta = a/b$ , for reasons that will be become evident soon. In this case, the GBZ and energy satisfy

$$\begin{aligned} \text{GBZ}_{2D,2} &= \left\{ z_x^{\alpha+\beta} z_y^{a+b} = \frac{t' \sin bk}{t \sin ak} e^{i(a+b)k} \mid k = \left(-\frac{\pi}{a+b}, \frac{\pi}{a+b}\right) \right\}, \\ \bar{E}(k) &= E(z_x, z_y) = \left( \frac{tbt'^a}{(\sin(ak))^a (\sin(bk))^b} \right)^{\frac{1}{a+b}} \sin((a+b)k) e^{\frac{2i\pi av}{a+b}}, \end{aligned} \quad (\text{S18})$$

with  $k = \left(-\frac{\pi}{a+b}, \frac{\pi}{a+b}\right]$  and  $v = 1, 2, \dots, a + b$ , as plotted in FIG. S3 (a–c). As this case only contains the combination  $z_x^{\alpha+\beta} z_y^{a+b}$ , rather than  $z_x^{\alpha+\beta}$  and  $z_y^{a+b}$ , it is essentially a 1D model along the  $\alpha\mathbf{x} + a\mathbf{y}$  direction, which is consistent with the results of numerical diagonalization as shown in FIG. S3(a1–a3).

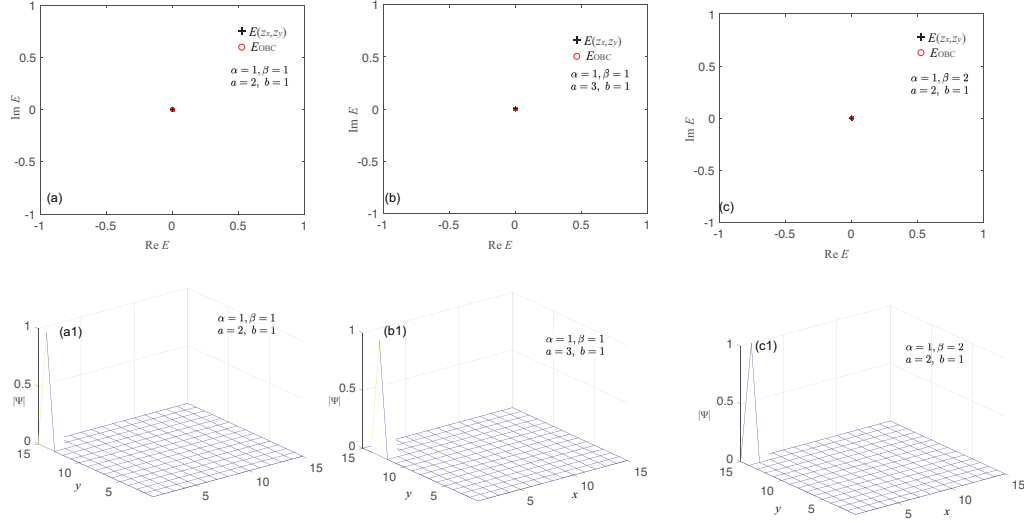


FIG. S2. Spectra and corner-localized eigenstates for  $H_{2D,2}$  in the  $\alpha/\beta \neq a/b$  case. (a–c) Exactly zero (flatband) OBC eigenenergies  $E_{OBC}$  due to non-Bloch collapse, which coincide with  $E(z_x, z_y)$  from Eq.(S19). (a1–c1) Corresponding illustrative eigenstates are perfectly localized at the boundary dictated by the direction of localization. The model parameters are  $L_x = L_y = 15$ ,  $t = 2$ ,  $t' = 1$  and the specific values of  $\alpha, \beta, a, b$  are indicated in the figure.

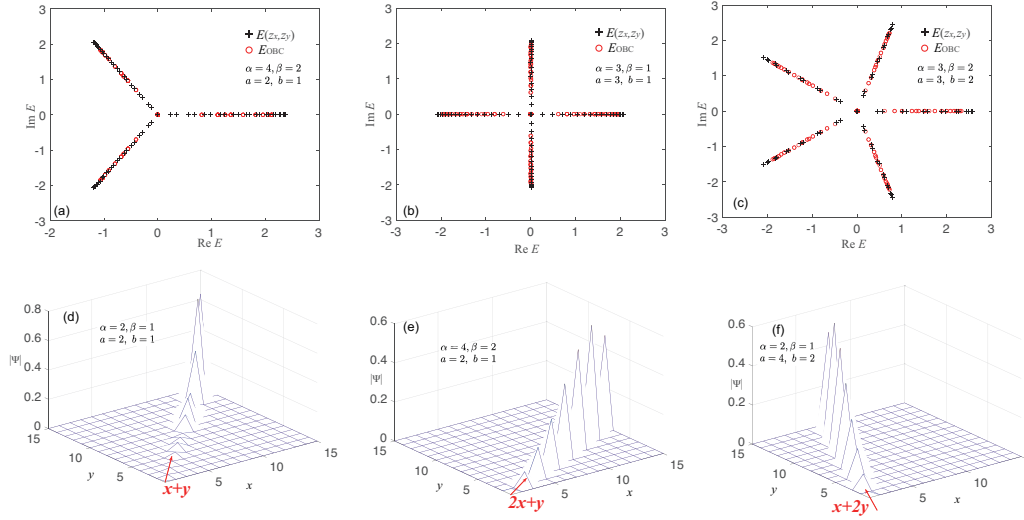


FIG. S3. Spectra and illustrative eigenstates for  $H_{2D,2}$  in the  $\alpha/\beta = a/b$  case. (a–c) Excellent agreement between the GBZ eigenenergies  $E(z_x, z_y)$  from Eq.(S18) and OBC eigenenergies  $E_{OBC}$  of Eq.(S13). (d–f) Spatial profiles for the  $E_{OBC} = 0$  eigenstate of a few other illustrative cases, clearly showing that the skin states are aligned along the  $\alpha\hat{x} + a\hat{y}$  (or  $\beta\hat{x} + b\hat{y}$ ) direction. The model parameters are  $L_x = L_y = 15$ ,  $t = 1$ ,  $t' = 2$  and the specific values of  $\alpha, \beta, a, b$  are indicated in the figure.

We next discuss the other case with  $\alpha/\beta \neq a/b$ , where  $|z_1|$  and  $|z_2|$  can only coincide at  $z_1^{\alpha+\beta} = z_2^{\alpha+b} = -1$ . Hereby, its GBZ and energy are simply given by

$$\text{GBZ}_{2D,2} = \left\{ z_x^{\alpha+\beta} z_y^{\alpha+b} = -\frac{t'}{t} \right\}, \quad (S19)$$

$$E(z_x, z_y) = 0,$$

As confirmed in FIG. S2(a–c), the eigenenergies are indeed zero, and the eigenstates (FIG. S2(a1–c1)) are perfectly localized at a corner determined by  $\alpha/\beta, a/b$  and  $t/t'$ . This is because of uncompensated unbalanced hoppings along at least one direction, which leads to non-Bloch collapse [93, 155]. Since there is no nontrivial dynamics to speak of in this case, we shall not discuss it further.

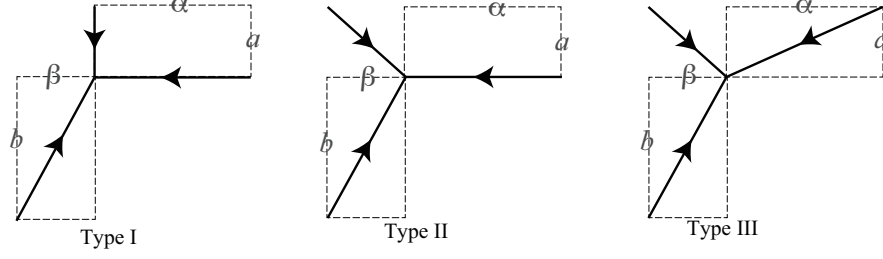


FIG. S4. The three directed hopping configurations in each of our type I,II and III models. For type I, two hoppings are orthogonal; for type II, two hoppings have common  $\beta$  displacements in the direction antiparallel to the third hopping; for type III, there exists two common  $\beta$  component displacements orthogonal to the two common  $a$  displacements.

## 2D lattice model with 3 hopping terms

We next discuss 2D lattices with 3 unbalanced hopping terms, such that their combined effect is no longer either trivial or just that along a 1D subspace. We shall study two types of hopping configurations here, and reserve the third type, which turns out to interestingly requires a GBZ of lower dimensionality, to the next section on its own.

*Type I: 2D lattice model with 3 hopping terms, 2 perpendicular to each other*

We first consider type I models, the simplest of “entangled” 2D lattice models. They contain 2 perpendicular terms  $t_1, t_2$  in directions  $(\alpha, 0)$  and  $(0, a)$ , and a third one in an oblique direction  $-(\beta, b)$ . We have

$$H_{2D,I} = \sum_{m,n} t_1 |m, n\rangle \langle m + \alpha, n| + t_2 |m, n\rangle \langle m, n + a| + t_3 |m, n\rangle \langle m - \beta, n - b|. \quad (\text{S20})$$

Similarly as before, by substituting the ansatz  $|\psi\rangle \propto \sum_{m,n} \psi_{mn} |m, n\rangle$  with  $\psi_{m,n} = z_x^m z_y^n$  into the bulk equations, we obtain the energy  $E(z_x, z_y)$

$$E(z_x, z_y) = t_1 z_x^\alpha + t_2 z_y^a + t_3 z_x^{-\beta} z_y^{-b}. \quad (\text{S21})$$

By heuristically regarding  $E(z_x, z_y)$  as 1D models  $E(z_x)$  or  $E(z_y)$  with nonconstant hoppings and using Eqs. S11 and S12, or by considering boundary conditions on the wave function  $|\Psi\rangle$  (Eq.(S15)), we obtain the following relationships between  $z_x$  and  $z_y$ :

$$\begin{aligned} z_x^{\alpha+\beta} z_y^b &= \frac{t_3}{t_1} z_1^{\alpha+\beta}, & z_1^{\alpha+\beta} &= \frac{\sin \beta k_1}{\sin \alpha k_1} e^{i(\alpha+\beta)k_1}, & k_1 &\in \left( -\frac{\pi}{\alpha+\beta}, \frac{\pi}{\alpha+\beta} \right], \\ z_x^\beta z_y^{a+b} &= \frac{t_3}{t_2} z_2^{a+b}, & z_2^{a+b} &= \frac{\sin b k_2}{\sin a k_2} e^{i(a+b)k_2}, & k_2 &\in \left( -\frac{\pi}{a+b}, \frac{\pi}{a+b} \right]. \end{aligned} \quad (\text{S22})$$

Substituting these  $z_x$  and  $z_y$  into the energy expression Eq.(S21), we obtain the GBZ energies (Note the slight abuse of notation - below, we write  $E(z_x, z_y) = E(z_1, z_2)$  to convey that the set of  $E$  depends on  $z_1, z_2$  through  $z_x, z_y$ , even though  $E$  of course takes different functional dependencies in either case. )

$$\bar{E}(k_1, k_2) = E(z_x, z_y) = \left( \frac{t_1^\beta t_2^\alpha t_3^\alpha}{z_1^{(\alpha+\beta)a\beta} z_2^{(a+b)b\alpha}} \right)^{\frac{1}{(\alpha+\beta)a+\alpha b}} \times \left( 1 + z_1^{\alpha+\beta} + z_2^{a+b} \right), \quad (\text{S23})$$

and

$$\text{GBZ}_{2D,I} = \left\{ z_x, z_y \left| z_x^{(\alpha+\beta)a+\alpha b} = \frac{t_2^\beta t_3^\alpha}{t_1^{a+b}} \frac{z_1^{(\alpha+\beta)(a+b)}}{z_2^{(a+b)b}}, z_y^{(\alpha+\beta)a+\alpha b} = \frac{t_1^\beta t_3^\alpha}{t_2^{\alpha+\beta}} \frac{z_2^{(\alpha+\beta)(a+b)}}{z_1^{(\alpha+\beta)\beta}} \right. \right\}, \quad (\text{S24})$$

with  $z_1, z_2$  functions of  $k_1, k_2$ , as defined in Eq.(S22). Some comments on the relationship between  $z_x, z_y$  and  $z_1, z_2$  are in order. As defined by the ansatz  $|\psi(x, y)\rangle \propto \sum_{m,n} z_x^m z_y^n |m, n\rangle$ ,  $z_x, z_y$  control the spatial growth and decay of

the wavefunction. However, unlike in an “unentangled” case like  $H_{2D,2}$ , both  $z_x$  and  $z_y$  depend on the GBZ spanning parameters  $k_1, k_2$  in complicated manners given by Eq. S22. In other words, Eq. S22 dictates how the “non-Bloch” scaling factors  $z_x, z_y$  are related to the GBZ coordinates  $k_1, k_2$  through intermediate quantities  $z_1, z_2$ , which are related to the effective 1D chain projections of the Hamiltonian.

From this explicit expression Eq. S24, we can already deduce that the locus of  $E$  is a star-like set of branches, since  $E$  factorizes into a product of terms involving the phase factors of  $k_1$  and  $k_2$  separately. By considering these phase factors, we find that the number of branches for a type-I hopping lattice is given by

$$\text{LCM} \left[ \frac{(\alpha + \beta)a + \alpha b}{\text{GCD}((\alpha + \beta)a + \alpha b, (\alpha + \beta)a\beta)}, \frac{(\alpha + \beta)a + \alpha b}{\text{GCD}((\alpha + \beta)a + \alpha b, (a + b)\alpha b)} \right]. \quad (\text{S25})$$

Their agreement with numerical OBC results is given in FIG. S5. The phase factor is given by  $\exp\left(\frac{2\pi i((\alpha + \beta)a\beta k_1 + (a + b)\alpha b k_2)}{(\alpha + \beta)a + \alpha b}\right)$ , which evaluates to  $\exp\left(\frac{2\pi i(2k_1 + 2k_2)}{3}\right) \Leftrightarrow 3$  branches for (a4);  $\exp\left(\frac{2\pi i(3k_1 + 4k_2)}{5}\right) \Leftrightarrow 5$  branches for (b4); and  $\exp\left(\frac{2\pi i(3k_1 + 12k_2)}{7}\right) \Leftrightarrow 7$  branches for (c4).

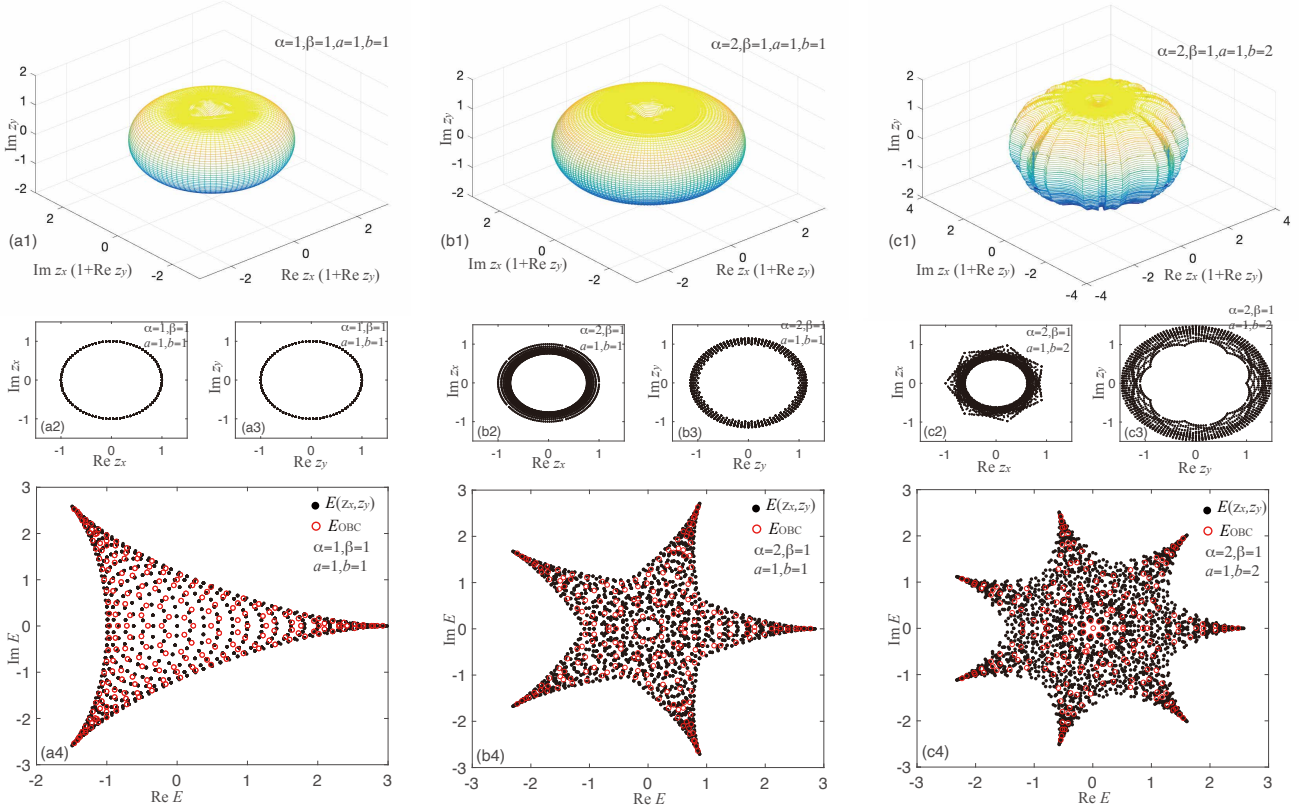


FIG. S5. Plots of the GBZ torus (Upper row a1-c1), GBZs  $z_x$  (Middle row a2-c2) and  $z_y$  (Middle row a3-c3), as well as the energy spectra (Lower row a4-c4) of illustrative type-I lattices ( $H_{2D,I}$  from Eq. (S20)) with hoppings given by parameters  $\alpha, \beta, a, b$ . The upper row plots (a1-c1) are parametrized such that a torus is traced out in the trivial case without NHSE ( $|z_x| = |z_y| = 1$  for all  $k_1, k_2$ ); departures from a toroidal shape depict the extent of 2D NHSE. Belonging to a 2D model, each of  $z_x, z_y$  (a1-c1, a2-c2, a3-c3), traces out a 2D region parametrized by  $k_1, k_2$  (Eq. S24) as its GBZ, even though it trivially collapses into 1D loops for case (a). Perfect agreement of GBZ spectra  $E(z_x, z_y)$  from Eq. (S23) with OBC spectra  $E_{\text{OBC}}$  is demonstrated for all cases, which for this model fills the interior of a  $[(\alpha + \beta)a + \alpha b]$ -sided figure (a4-c4). Parameters are  $L_x = L_y = 15$ ,  $t_1 = t_2 = t_3 = 1$ , and the GBZ predictions are generated with a mesh defined by  $k_1 = -\frac{\pi}{\alpha + \beta} : \frac{\pi}{30} : \frac{\pi}{\alpha + \beta}$ ,  $k_2 = -\frac{\pi}{a + b} : \frac{\pi}{30} : \frac{\pi}{a + b}$ .

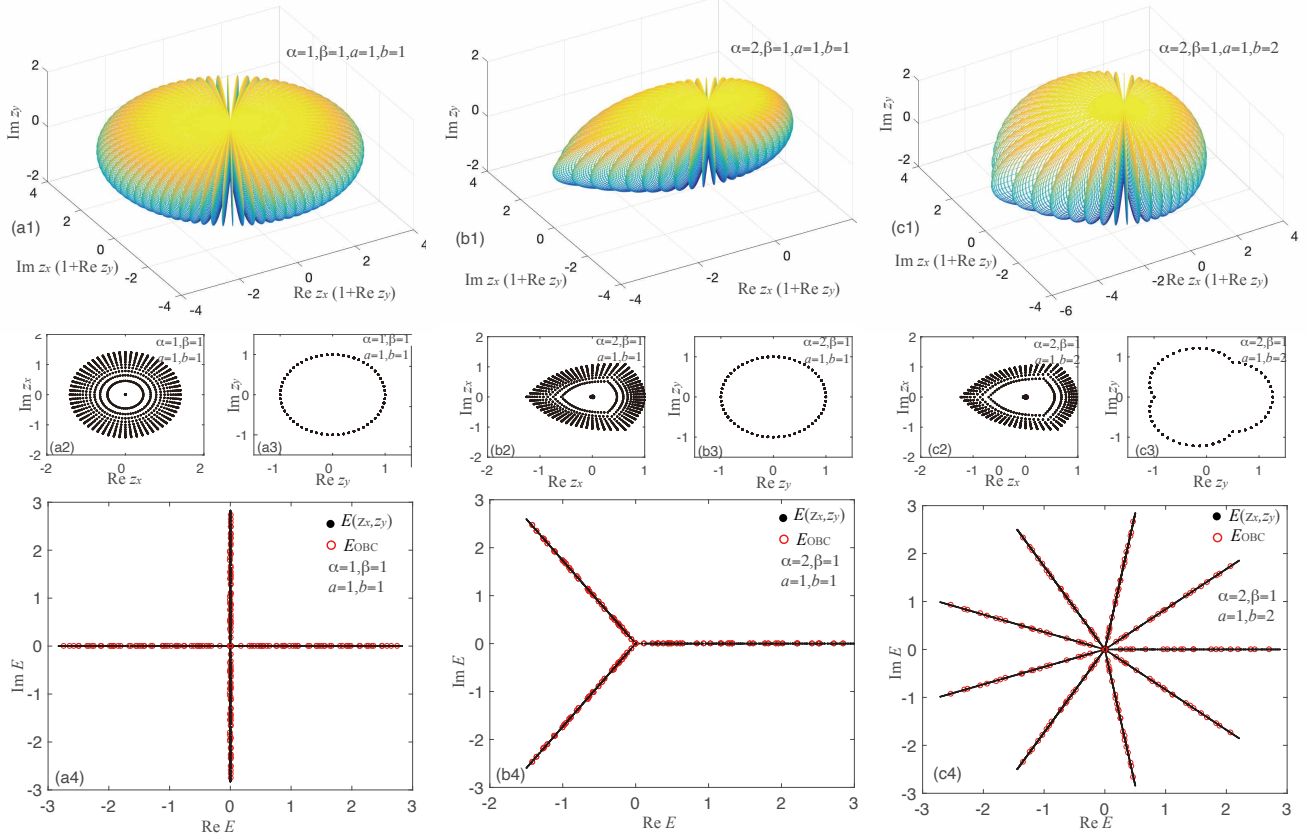
Type II: 2D lattice model with 3 hopping terms, two with common  $\beta$  displacement

FIG. S6. Plots of the GBZ torus (Upper row a1-c1), GBZs  $z_x$  (Middle row a2-c2) and  $z_y$  (Middle row a3-c3), as well as the energy spectra (Lower row a3-c3) of illustrative type-II lattices ( $H_{2D,II}$  from Eq. (S26)) with hoppings given by parameters  $\alpha, \beta, a, b$ . (a1-c1, a2-c2, a3-c3) While  $z_x$  traces out a 2D region parametrized by the two “momenta”  $k_1$  and  $k_2$ ,  $z_y$  only depends on one such momentum parameter, as given by Eq. (S28), thereby tracing out a 1D GBZ loop (a3-c3). (a4-c4) Perfect agreement of GBZ spectra  $E(z_x, z_y)$  from Eq. (S27) with OBC spectra  $E_{OBC}$  is demonstrated for all cases, with their star-like spectra consistent with the 1D nature of their effective GBZ description. The  $|z_x| = 0$  central dot corresponds to  $k_2 = \pm\pi/(a+b)$  where the factor  $(z_2^a + z_2^{-b})$  in  $z_x$  is equal to 0. Parameters are  $L_x = L_y = 15$ ,  $t_1 = t_2 = t_3 = 1$ , and the GBZ predictions are generated with a mesh defined by  $k_1 = -\frac{\pi}{\alpha+\beta} : \frac{\pi}{\alpha+\beta}$ ,  $k_2 = -\frac{\pi}{a+b} : \frac{\pi}{a+b}$ .

We next consider a slightly more complicated 2D lattice model (type II). None of the hoppings are orthogonal to each other, so all 3 hoppings are “entangled”. However, it has the simplifying property that the  $t_2$  and  $t_3$  hoppings are equidistant in the direction parallel to the  $t_1$  hopping, such that if we set the  $t_1$  hopping normal against the horizontal  $x$  open boundary, there are only two unique hopping distances in this direction. The Hamiltonian is given by

$$H_{2D,II} = \sum_{m,n} t_1 |m,n\rangle \langle m+\alpha, n| + t_2 |m,n\rangle \langle m-\beta, n+a| + t_3 |m,n\rangle \langle m-\beta, n-b|. \quad (S26)$$

Taking the ansatz  $|\psi\rangle \propto \sum_{m,n} \psi_{mn} |m,n\rangle$  with  $\psi_{m,n} = z_x^m z_y^n$  into the bulk equations, we obtain the energy  $E(z_x, z_y)$

$$E(z_x, z_y) = t_1 z_x^\alpha + t_2 z_x^{-\beta} z_y^a + t_3 z_x^{-\beta} z_y^{-b}. \quad (S27)$$

Considering the boundary conditions in the same way as before, we have two relations between  $z_x$  and  $z_y$  from which the GBZ and OBC energy  $E(z_x, z_y)$  can be obtained:

$$\text{GBZ}_{2D,II} = \left\{ z_x, z_y \left| z_x^{\alpha+\beta} = t_1^{-1} t_2^{\frac{b}{\alpha+\beta}} t_3^{\frac{a}{\alpha+\beta}} (z_2^a + z_2^{-b}) z_1^{\alpha+\beta}, z_y^{a+b} = \frac{t_3}{t_2} z_2^{a+b} \right. \right\}, \quad (S28)$$

$$\bar{E}(k_1, k_2) = E(z_x, z_y) = t_1^{\frac{\beta}{\alpha+\beta}} \left( t_2^{\frac{b}{\alpha+\beta}} t_3^{\frac{a}{\alpha+\beta}} (z_2^a + z_2^{-b}) \right)^{\frac{\alpha}{\alpha+\beta}} (z_1^\alpha + z_1^{-\beta}), \quad (\text{S29})$$

the forms of  $z_1, z_2$  given in Eq.(S22) as before.

From the explicit expression Eq. S29, we can similarly deduce that the locus of  $E$  is a star-like set of branches. We find that the number of branches for type-II lattice hoppings is given by

$$\text{LCM} \left[ \frac{(a+b)(\alpha+\beta)}{\text{GCD}((a+b)(\alpha+\beta), a\alpha)}, \frac{\alpha+\beta}{\text{GCD}(\alpha+\beta, \alpha)} \right]. \quad (\text{S30})$$

We verify this formula with the three examples in FIG. S6, for which there exist excellent agreement between the numerical OBC results and the above GBZ expression for  $E$ . The phase factor is given by  $\exp\left(\frac{2\pi(a\alpha k_1 + \alpha(a+b)k_2)}{(a+b)(\alpha+\beta)}\right)$ , which evaluates to  $\exp\left(\frac{2\pi i(k_1+2k_2)}{4}\right) \Leftrightarrow 4$  branches for (a4);  $\exp\left(\frac{2\pi i(k_1+k_2)}{6/2}\right) \Leftrightarrow 3$  branches for (b4); and  $\exp\left(\frac{2\pi(2k_1+6k_2)}{9}\right) \Leftrightarrow 9$  branches for (c4). It is not surprising that these type II 2D lattice models considered above have star-like spectra that resemble that of 1D NHSE models, since they after quickly reduce to a simple 1D effective model with x-OBCs with 2 effective hoppings.

## 2D LATTICES WITH DIMENSIONALLY-REDUCED GBZS

The previous section gives the approach to obtain the GBZ of 2D lattice models. However, as explained in the main text, there are some classes of models where the correct GBZ is not even of the same dimensionality as the lattice. In this section, we shall provide a detailed account of the additional steps and analysis required to dimensionally reduce the GBZ to the correct one.

### Model description and setup

We consider 2D lattice models of the form (type III in Fig. S4)

$$H_{2D,III} = \sum_{m,n} t_1 |m, n\rangle \langle m + \alpha, n + a| + t_2 |m, n\rangle \langle m - \beta, n + a| + t_3 |m, n\rangle \langle m - \beta, n - b|, \quad (S31)$$

with oblique hoppings of amplitudes  $t_1, t_2, t_3$ . They constitute minimal models that require dimensional reduction of the GBZ, and are still simple enough such that they can be analyzed completely analytically. Using the ansatz  $|\psi\rangle \propto \sum_{m,n} \psi_{mn} |m, n\rangle$  with  $\psi_{m,n} = z_x^m z_y^n$  as before, the bulk relations give  $t_1 \psi_{m+\alpha, n+a} + t_2 \psi_{m-\beta, n+a} + t_3 \psi_{m-\beta, n-b} = E(z_x, z_y) \psi_{m,n}$ , which yields

$$E(z_x, z_y) = t_1 z_x^\alpha z_y^a + t_2 z_x^{-\beta} z_y^a + t_3 z_x^{-\beta} z_y^{-b}. \quad (S32)$$

By treating the system as a quasi-1D system in  $x$  or  $y$  as before i.e. by expressing it in the form of Eq. S1 with GBZ and energies given by Eqs. S11 and S12, we obtain

$$z_x^{\alpha+\beta} = \frac{t_2 + t_3 z_y^{-a-b}}{t_1} z_1^{\alpha+\beta}, \quad z_1^{\alpha+\beta} = \frac{\sin \beta k_1}{\sin \alpha k_1} e^{i(\alpha+\beta)k_1}, \quad k_1 \in \left( -\frac{\pi}{\alpha + \beta}, \frac{\pi}{\alpha + \beta} \right], \quad (S33)$$

and

$$z_y^{a+b} = \frac{t_3}{t_1 z_x^{\alpha+\beta} + t_2} z_2^{a+b}, \quad z_2^{a+b} = \frac{\sin b k_2}{\sin a k_2} e^{i(a+b)k_2}, \quad k_2 \in \left( -\frac{\pi}{a + b}, \frac{\pi}{a + b} \right]. \quad (S34)$$

That is, the boundary conditions along the two different direction give us two relations on  $z_x$  and  $z_y$  respectively. In order to get  $z_x, z_y$  which satisfy all the boundary conditions, we solve the above to obtain

$$z_x^{\alpha+\beta} = \frac{t_2}{t_1} \frac{1 + z_2^{a+b}}{z_2^{a+b} - z_1^{\alpha+\beta}} z_1^{\alpha+\beta}, \quad z_y^{a+b} = \frac{t_3}{t_2} \frac{z_2^{a+b} - z_1^{\alpha+\beta}}{1 + z_1^{\alpha+\beta}}. \quad (S35)$$

Note that now,  $z_x$  and  $z_y$  are not even proportional to a single phase factor, and thus no longer take any conventional “non-Bloch” form. Substituting  $z_x, z_y$  Eq.(S35) into the energy  $E(z_x, z_y)$  Eq.(S32), we furthermore obtain

$$\bar{E}(k_1, k_2) = E(z_x, z_y) = \frac{\left( t_1^\beta (1 + z_2^{a+b})^\alpha \right)^{\frac{1}{\alpha+\beta}} \cdot \left( t_3^a (1 + z_1^{\alpha+\beta})^b \right)^{\frac{1}{a+b}}}{\left( (z_2^{a+b} - z_1^{\alpha+\beta}) / t_2 \right)^{\frac{\alpha b - \beta a}{(\alpha+\beta)(a+b)}}} z_1^{-\beta}, \quad (S36)$$

with  $v = 1, 2, \dots, a + b$ , the forms of  $z_1, z_2$  given by Eq.(S33 and S34).

Importantly, this 2D GBZ ( $z_x, z_y$ ) as it is currently defined does *not* form a valid GBZ because there exists certain paths on it where the spectral winding

$$\omega_i(E) = \oint dz_i \partial_{z_i} \log(E(\mathbf{k}) - E_0), \quad (S37)$$

$i = 1, 2$  is nonzero for some arbitrary reference energies  $E_b$ . In other words, there exist some closed paths in  $(k_1, k_2)$  space (defined in Eqs. S33, S34) such that the energy  $E(k_1, k_2)$  loop encloses a nonzero area as we cycle over  $k_1$  or  $k_2$ . An illustrative example is shown in Fig. S7.

Since it is known[89, 95] that OBC spectra should never possess nonzero spectral winding, which presupposes incomplete NHSE equilibration, the above results Eqs. S35 and S36 cannot possibly give the correct OBC spectrum

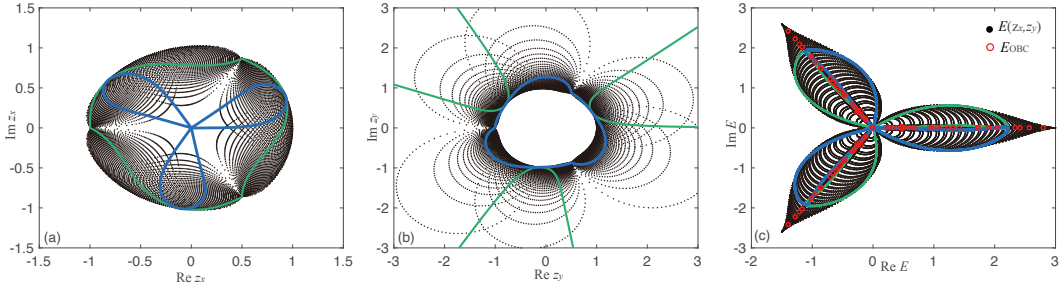


FIG. S7. (a,b) Closed paths from the unconstrained GBZ from Eq. S33 to S35 that result in nontrivial spectral winding, in contradiction to the known fact that OBC spectra should not enclose any nonzero area (nontrivial winding). The unconstrained GBZ  $z_x$  (a) and  $z_y$  (b) of  $H_{2D,III}$  with  $t_1 = t_2 = t_3 = 1$  are plotted in black for  $k_1, k_2$  ranging over all values in steps of  $\pi/100$ , with illustrative green and blue closed paths enclosing nonzero area given by  $k_1 = (-\pi/3, \pi/3), k_2 = \pi/6$  and  $k_2 = (-\pi/3, \pi/3), k_1 = \pi/6$  respectively. (c) The corresponding spectrum (Eq. S36) from the unconstrained GBZ (black) and the corresponding green and blue spectral loops that enclose non-vanishing areas, which they are not supposed to do. In particular, they do not agree with the correct, numerically obtained OBC spectrum (red), which lies on a subset of  $E(z_x, z_y)$  points, but which does not exhibit any nontrivial winding.

of  $H_{2D, III}$ . Indeed, this is shown in the lack of agreement between the numerically obtained  $E_{OBC}$  spectrum and the (currently unconstrained) GBZ spectrum  $E(z_x, z_y)$  in Fig. S7. Yet, the above results can be rigorously traced to satisfy all the relations pertaining to the real-space hoppings, and cannot be incorrect. Hence the natural conclusion is that the correct GBZ must be a subset of the GBZ, as currently defined by Eqs. S33 to S35 with the range of  $k_1, k_2$  prescribed above. In the below, we shall carefully derive the constraints that extracts the subset of  $k_1, k_2$  that generates the correct GBZ for this model; at the end of this supplement, we shall generalize this correct GBZ construction to arbitrary non-Hermitian lattice models.

### Detailed analysis of constraints leading to dimensional reduction

Here, we elaborate on the possible constraints that can make the energy spectrum (Eq. S36) exhibit zero winding. Since the unconstrained GBZ is a 2D torus that is spanned by 2 homotopy generators, a sure way to remove all possible nonzero spectral windings is to remove the homotopy generator/s that lead to particular nontrivial spectral winding paths. In principle, there can be many ways to remove a homotopy generator, since a combination of generators form another generator. However, for our model  $H_{2D,III}$ , it turns out that the requisite constraints can simply take the linear form of  $k_1 = \gamma k_2$ , with  $\gamma$  taking particular values that we shall elaborate on. (Note that we cannot possibly remove both homotopy generators, since there will be no GBZ left then.)

#### Analysis of different possible parametrizations

We now justify why it suffices to consider  $k_1 = \gamma k_2$ , such that the energy takes the 1-parameter form  $\bar{E}(k_2)$  (or equivalently  $\bar{E}(k_1)$ ), with an slight abuse of notation. First, we establish the range and offset of  $k_1, k_2$ . given that  $z_1, z_2$  (Eqs. S33,S34) satisfy periodicity conditions  $z_1(k_1) = z_1(k_1 + 2m'\pi/(\alpha + \beta))$ ,  $z_2(k_2) = z_2(k_2 + 2n'\pi/(a + b))$  with integer  $n', m'$  ( $n', m' \in \mathbb{Z}$ ). We can hence write down a valid linear reparametrization as  $k_1 = \gamma k_2 + 2n'\pi\gamma/(a + b) + 2m'\pi/(\alpha + \beta)$  with integer  $n', m'$ , such that the energy Eq.(S36) is transformed into  $\bar{E}'$  as given by

$$\begin{aligned}
 \bar{E}' &= E(z_x, z_y) \Big|_{k_1 = \gamma k_2 + \frac{2n'\pi\gamma}{a+b} + \frac{2m'\pi}{\alpha+\beta}} = E(z_1(k_1), z_2(k_2)) \Big|_{k_1 = \gamma k_2 + \frac{2n'\pi\gamma}{a+b} + \frac{2m'\pi}{\alpha+\beta}} \\
 &= E(z_1(\gamma k_2 + 2n'\pi\gamma/(a + b)), z_2(k_2)) \\
 &= \bar{E} \left( k_2 + \frac{2n'\pi}{a + b} \right),
 \end{aligned} \tag{S38}$$

such as  $E' \in \{E(k_2)\}$ . Since this hence just a translation of a single coordinate, we can hence just consider constraints of the form  $k_1 = \gamma k_2$  without any constant offset. With that,

$$\bar{E}(k_2) = E(z_x, z_y) \Big|_{k_1=\gamma k_2} = E(z_1(k_1), z_2(k_2)) \Big|_{k_1=\gamma k_2} = E(z_1(\gamma k_2), z_2(k_2)) . \quad (\text{S39})$$

Next, we shall show that there exists 3 possible values of  $\gamma$  that guarantee zero spectral winding number while keeping  $z_x, z_y$  periodic, namely  $\gamma = b/\beta$ ,  $a/\alpha$ ,  $(a+b)/(\alpha+\beta)$ . Below are the detailed justifications for the possible choices of  $\gamma$  (we call them  $\gamma_1, \gamma_2$  and  $\gamma_3$ ):

- The case with  $k_1 = \gamma_1 k_2$ ,  $\gamma_1 = b/\beta$ : Here  $z_x, z_y$  (S35) and energy (S36) with  $k_1 = bk, k_2 = \beta k$  are given by

$$\begin{aligned} z_{x,1}^{\alpha+\beta} &= z_x^{\alpha+\beta} \Big|_{k_1=\gamma_1 k_2} = \frac{t_2 \sin((a+b)\beta k)}{t_1 \sin((\alpha b - a\beta)k)} e^{i(\alpha b + \beta b)k} , \\ z_{y,1}^{a+b} &= z_y^{a+b} \Big|_{k_1=\gamma_1 k_2} = \frac{t_3 \sin(\beta b k) \sin((\alpha b - a\beta)k)}{t_2 \sin(a\beta k) \sin((\alpha b + \beta b)k)} , \end{aligned} \quad (\text{S40})$$

$$\begin{aligned} \bar{E}_1(k) &= E(z_x, z_y) \Big|_{k_1=\gamma_1 k_2=bk} , \\ &= t_1^{\frac{\beta}{\alpha+\beta}} t_2^{\frac{\alpha b - \beta a}{(\alpha+\beta)(a+b)}} t_3^{\frac{a}{\alpha+\beta}} e^{\frac{i2\pi a v}{\alpha+\beta} + \frac{2\pi \alpha v'}{\alpha+\beta}} \left( \frac{\sin(\alpha b + \beta b)k}{\sin \alpha b k} \right)^{\frac{b}{\alpha+\beta}} \\ &\quad \times \left( \frac{\sin(a\beta + \beta b)k}{\sin a\beta k} \right)^{\frac{\alpha}{\alpha+\beta}} \left( \frac{\sin \beta b k}{\sin \alpha b k} \right)^{-\frac{\beta}{\alpha+\beta}} \left( \frac{\sin(a+b)\beta k}{\sin a\beta k} - \frac{\sin(\alpha b + \beta b)k}{\sin \alpha b k} \right)^{\frac{\beta a - \alpha b}{(\alpha+\beta)(a+b)}} , \end{aligned} \quad (\text{S41})$$

where  $v = 1, 2, \dots, a+b$ ,  $v' = 1, 2, \dots, \alpha+\beta$ . The range of  $k$  has to be dependent on the ratio between  $\alpha/\beta$  and  $a/b$  as follows:

- $\alpha/\beta > a/b$ :  $k$  can take values in  $\left(-\frac{\pi}{(\alpha+\beta)b}, \frac{\pi}{(\alpha+\beta)b}\right]$ . Both  $z_{x,1}$  and  $z_{y,1}$  are connected end to end with ‘momentum’  $k$ , and the path of  $z_{x,1}$  in the complex plane forms a closed loop. Hence, the results of  $z_{x,1}, z_{y,1}$  (Eq.(S40)) are legitimate, and zero winding in the energy  $\bar{E}_1$  (Eq.(S41)) is respected.
- $\alpha/\beta = a/b$ :  $k$  can take values in  $\left(-\frac{\pi}{(a+b)\beta}, \frac{\pi}{(a+b)\beta}\right]$ . And  $z_{x,1}^{\alpha+\beta} \rightarrow \infty$ ,  $z_{y,1}^{a+b} \rightarrow 0$ , but the path of  $z_{x,1}^{\alpha+\beta} z_{y,1}^{a+b} = \frac{\sin(\beta b k)}{\sin(a\beta k)} e^{i(a+b)\beta k}$  in the complex plane forms a closed loop with ‘momentum’  $k$ . Hence, the results of  $z_{x,1}, z_{y,1}$  Eq.(S40) are legitimate, and zero winding in the energy  $\bar{E}_1$  Eq.(S41) is respected.
- $\alpha/\beta < a/b$ :  $k$  can take values in  $\left(-\frac{\pi}{(a+b)\beta}, \frac{\pi}{(a+b)\beta}\right]$ . None of  $z_{x,1}^{\alpha+\beta}$ ,  $z_{y,1}^{a+b}$ ,  $z_{x,1}^{\alpha+\beta} z_{y,1}^{a+b}$  can form closed loop parametrized by ‘momentum’  $k$ . The results of  $z_{x,1}, z_{y,1}$  and the zero winding requirement of the energy  $\bar{E}_1$  Eq.(S41) are inconsistent. It is worth noting that when  $z_1^{\alpha+\beta} = z_2^{a+b}$  in Eq.(S35), the  $z_x^{\alpha+\beta} \rightarrow \infty, z_y^{a+b} \rightarrow 0$  which can ignore the end-to-end condition. And in this case, the energy  $\bar{E} = 0$ .

- The case with  $k_1 = \gamma_2 k_2$ ,  $\gamma_2 = a/\alpha$ :  $z_x, z_y$  (S35) and the energy (S36) with  $k_1 = ak', k_2 = \alpha k'$  are given by

$$\begin{aligned} z_{x,2}^{\alpha+\beta} &= z_x^{\alpha+\beta} \Big|_{k_1=\gamma_2 k_2} = \frac{t_2 \sin(\beta a k') \sin((\alpha a + \alpha b)k')}{t_1 \sin(a\alpha k') \sin((\alpha b - \beta a)k')} , \\ z_{y,2}^{a+b} &= z_y^{a+b} \Big|_{k_1=\gamma_2 k_2} = \frac{t_3 \sin((\alpha b - a\beta)k')}{t_2 \sin((\alpha a + a\beta)k')} e^{i(\alpha a + \alpha b)k'} , \end{aligned} \quad (\text{S42})$$

$$\begin{aligned} \bar{E}_2(k') &= E(z_x, z_y) \Big|_{k_1=\gamma_2 k_2=ak'} , \\ &= t_1^{\frac{\beta}{\alpha+\beta}} t_2^{\frac{\alpha b - \beta a}{(\alpha+\beta)(a+b)}} t_3^{\frac{a}{\alpha+\beta}} e^{\frac{i2\pi a v}{\alpha+\beta} + \frac{2\pi \alpha v'}{\alpha+\beta}} \left( \frac{\sin(\alpha a + \beta a)k'}{\sin \alpha a k'} \right)^{\frac{b}{\alpha+\beta}} \\ &\quad \times \left( \frac{\sin(a\alpha + \alpha b)k'}{\sin a\alpha k'} \right)^{\frac{\alpha}{\alpha+\beta}} \left( \frac{\sin \beta a k'}{\sin \alpha a k'} \right)^{-\frac{\beta}{\alpha+\beta}} \left( \frac{\sin(\alpha b - a\beta)k'}{\sin \alpha a k'} \right)^{\frac{\beta a - \alpha b}{(\alpha+\beta)(a+b)}} , \end{aligned} \quad (\text{S43})$$

where  $v = 1, 2, \dots, a+b$ ,  $v' = 1, 2, \dots, \alpha+\beta$ . The range of  $k'$  similarly has to depend on the ratio between  $\alpha/\beta$  and  $a/b$ :

- $\alpha/\beta > a/b$ ,  $k'$  can take values in  $\left(-\frac{\pi}{(a+b)\alpha}, \frac{\pi}{(a+b)\alpha}\right]$ . Both  $z_{x,2}$  and  $z_{y,2}$  are connected end to end with ‘momentum’  $k$ , and the path of  $z_{y,2}$  in complex plane forms a closed loop. Hence, the results of  $z_{x,2}, z_{y,2}$  (Eq.(S42)) are legitimate, and zero winding in the energy  $\bar{E}_2$  Eq.(S43) is respected.
  - $\alpha/\beta = a/b$ ,  $k'$  can take values in  $\left(-\frac{\pi}{(a+b)\alpha}, \frac{\pi}{(a+b)\alpha}\right]$ . And  $z_{x,2}^{\alpha+\beta} \rightarrow \infty$ ,  $z_{y,2}^{a+b} \rightarrow 0$ , but the path of  $z_{x,2}^{\alpha+\beta} z_{y,2}^{a+b} = \frac{\sin(\alpha b k')}{\sin(\alpha a k')} e^{i(a+b)\alpha k'}$  in the complex plane forms a closed loop with ‘momentum’  $k$ . Hence, the results of  $z_{x,2}, z_{y,2}$  Eq.(S42) are legitimate, and zero winding in the energy  $\bar{E}_2$  Eq.(S43) is respected.
  - $\alpha/\beta < a/b$ ,  $k'$  can take values in  $\left(-\frac{\pi}{(\alpha+\beta)a}, \frac{\pi}{(\alpha+\beta)a}\right]$ . None of  $z_{x,2}^{\alpha+\beta}$ ,  $z_{y,2}^{a+b}$ ,  $z_{x,2}^{\alpha+\beta} z_{y,2}^{a+b}$  can form closed loop parametrized by ‘momentum’  $k'$ . The results of  $z_{x,2}, z_{y,2}$  and the zero winding requirement of the energy  $\bar{E}_2$  Eq.(S43) seem unreasonable. It is worth noting that when  $z_1^{\alpha+\beta} = z_2^{a+b}$  in Eq.(S35), the  $z_x^{\alpha+\beta} \rightarrow \infty, z_y^{a+b} \rightarrow 0$  which can ignore the end-to-end condition. And in this case, the energy  $\bar{E} = 0$ .
- The case with  $k_1 = \gamma_3 k_2$ ,  $\gamma_3 = (a+b)/(\alpha+\beta)$ :  $z_x, z_y$  (S35) and energy (S36) with  $k_1 = (a+b)k'', k_2 = (\alpha+\beta)k''$  take the forms

$$\begin{aligned} z_{x,3}^{\alpha+\beta} &= z_x^{\alpha+\beta} \Big|_{k_1=\gamma_3 k_2} = \frac{t_2 \sin(\beta(a+b)k'')}{t_1 \sin(\alpha b - \beta a)k''} e^{i b(\alpha+\beta)k''}, \\ z_{y,3}^{a+b} &= z_y^{a+b} \Big|_{k_1=\gamma_3 k_2} = \frac{t_3 \sin(\alpha b - \beta a)k''}{t_2 \sin(a(\alpha+\beta)k'')} e^{i \alpha(a+b)k''}, \end{aligned} \quad (\text{S44})$$

$$\begin{aligned} \bar{E}_3(k'') &= E(z_x, z_y) \Big|_{k_1=\gamma_3 k_2=(a+b)k''}, \\ &= t_1^{\frac{\beta}{\alpha+\beta}} t_2^{\frac{\alpha b - \beta a}{(\alpha+\beta)(a+b)}} t_3^{\frac{a}{a+b}} e^{\frac{i 3 \pi a v}{a+b} + \frac{3 \pi \alpha v'}{\alpha+\beta}} \left( \frac{\sin(\alpha+\beta)(a+b)k''}{\sin \alpha(a+b)k''} \right)^{\frac{b}{a+b}} \left( \frac{\sin(a+b)(\alpha+\beta)k''}{\sin a(\alpha+\beta)k''} \right)^{\frac{\alpha}{\alpha+\beta}} \\ &\quad \times \left( \frac{\sin \beta(a+b)k''}{\sin \alpha(a+b)k''} \right)^{-\frac{\beta}{\alpha+\beta}} \left( \frac{\sin b(\alpha+\beta)k''}{\sin a(\alpha+\beta)k''} - \frac{\sin \beta(a+b)k''}{\sin \alpha(a+b)k''} \right)^{\frac{\beta a - \alpha b}{(\alpha+\beta)(a+b)}}, \end{aligned} \quad (\text{S45})$$

where  $v = 1, 2, \dots, a+b$ ,  $v' = 1, 2, \dots, \alpha+\beta$ . Here, the range of  $k''$  is always  $\left(-\frac{\pi}{(\alpha+\beta)(a+b)}, \frac{\pi}{(\alpha+\beta)(a+b)}\right]$ .

- $\alpha/\beta \neq a/b$ : none of  $z_{x,3}^{\alpha+\beta}$ ,  $z_{y,3}^{\alpha+\beta}$ ,  $z_{x,3}^{\alpha+\beta} z_{y,3}^{\alpha+\beta}$  can form closed loop parametrized by momentum  $k''$ . Hence the results of  $z_{x,3}, z_{y,3}$  (Eq.(S44)) are inadmissible, since they are inconsistent with the zero winding requirement of the energy  $E_3$  Eq.(S45).
- $\alpha/\beta = a/b$ : this case is equivalent to the case  $k_1 = \gamma_1 k_2$  or  $k_1 = \gamma_2 k_2$  with  $\alpha/\beta = a/b$ .

Hence, the case with  $k_1 = \gamma_3 k_2$ ,  $\gamma_3 = (a+b)/(\alpha+\beta)$  can incorporate the cases with  $k_1 = \gamma_{1,2} k_2$  ( $\gamma_1 = b/\beta, \gamma_2 = a/\alpha$ ).

### Summary

To summarize, the (correct) constrained GBZ of  $H_{2D, III}$  of Eq.(S31) is not 2D, but is made up of one or more disconnected 1D loops as described above, depending on the hopping lengths  $\alpha, \beta, a, b$ . We call the effective Hamiltonian constrained to this reduced GBZ  $H_{2D\text{-red}}$ :

- When  $\alpha/\beta > a/b$ , the GBZ and spectrum consists of the union of the two sectors

$$\begin{aligned} \text{GBZ} &= \text{GBZ}_1 \cup \text{GBZ}_2, \\ \text{GBZ}_1 &= \left\{ z_{x,1}, z_{y,1} \mid k \in \left( -\frac{\pi}{(\alpha+\beta)b}, \frac{\pi}{(\alpha+\beta)b} \right] \right\}, \\ \text{GBZ}_2 &= \left\{ z_{x,2}, z_{y,2} \mid k' \in \left( -\frac{\pi}{(a+b)\alpha}, \frac{\pi}{(a+b)\alpha} \right] \right\}, \end{aligned} \quad (\text{S46})$$

$$\{\bar{E}\} = \{\bar{E}_1\} \cup \{\bar{E}_2\}, \quad (\text{S47})$$

TABLE I. Brief summary of admissible GBZs for our type III model (Eq. S31)  
(Shaded boxes represent valid contributing GBZ sectors)

	$\mathbf{k}_1 = \gamma_1 \mathbf{k}_2$ ( $\gamma_1 = \frac{b}{\beta}$ )	$\mathbf{k}_1 = \gamma_2 \mathbf{k}_2$ ( $\gamma_2 = \frac{a}{\alpha}$ )	$\mathbf{k}_1 = \gamma_3 \mathbf{k}_2$ ( $\gamma_3 = \frac{a+b}{\alpha+\beta}$ )
	$z_{x(y),1} = z_{x(y)} _{k_1=\gamma_1 k_2}$	$z_{x(y),2} = z_{x(y)} _{k_1=\gamma_2 k_2}$	$z_{x(y),3} = z_{x(y)} _{k_1=\gamma_3 k_2}$
$\alpha/\beta > a/b$	<b><math>z_{x,1}</math>: closed loop</b> $z_{y,1}$ : real	$z_{x,2}$ : real <b><math>z_{y,2}</math>: closed loop</b>	$z_{x,3}, z_{y,3}, z_{x,3}^{\alpha+\beta}, z_{y,3}^{\alpha+\beta}$ : open loop
Hence GBZ=GBZ <sub>1</sub> ∪ GBZ <sub>2</sub> (with GBZ <sub>1</sub> = { $z_{x,1}, z_{y,1}$ }, GBZ <sub>2</sub> = { $z_{x,2}, z_{y,2}$ })			
$\alpha/\beta = a/b$	$z_{i,1} = z_{i,2} = z_{i,3}$ ( $i = x, y$ ) and $z_{x,1} \rightarrow \infty, z_{y,1} \rightarrow 0$ <b><math>z_{x,1}^{\alpha+\beta}, z_{y,1}^{\alpha+b}</math>: closed loop</b>		
Hence GBZ = { $z_{x,1}^{\alpha+\beta}, z_{y,1}^{\alpha+b}$ }			
$\alpha/\beta < a/b$	$z_{x,j} \rightarrow \infty, z_{y,j} \rightarrow 0$ ( $j = 1, 2, 3$ ) $\bar{E} = 0$		

where the forms of  $z_{x(y),1(2)}$  can be found in Eq.(S40,S42) and that of  $E_{1,2}$  can be found in Eq.(S41,S43). Unlike with the unconstrained GBZ, they agree excellently with numerics, as shown in the example in FIG. S8. In other words, the effective surrogate OBC Hamiltonian of the case  $\alpha/\beta > a/b$  takes the form

$$\bar{H}_{2D\text{-red}} = \bar{H}_{2D,III} = \bar{H}_1 \oplus \bar{H}_2, \quad (\text{S48})$$

where  $\bar{H}_1$  and  $\bar{H}_2$  are the Hamiltonian operators with corresponding spectra  $\bar{E}_1$  and  $\bar{E}_2$  (Eqs. S41 and S43).

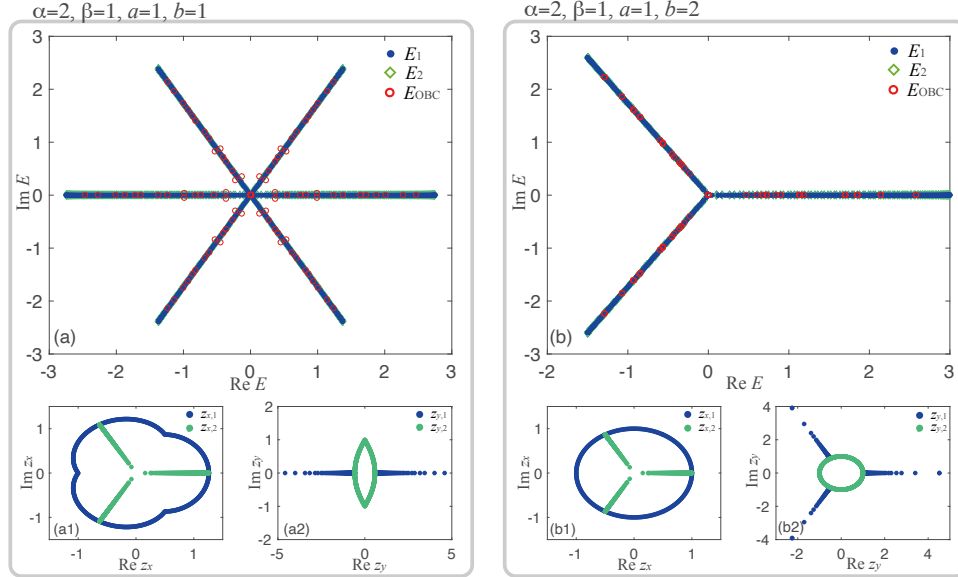


FIG. S8. The constrained GBZs and corresponding spectra  $\bar{E}$  of two illustrative cases of  $H_{2D, III}$  with hopping lengths  $\alpha/\beta > a/b$ , as indicated on top of the panels. Top) Coincident spectral contributions  $\bar{E}_1, \bar{E}_2$  from 1D GBZ sectors 1 and 2 of these 2D lattices, as defined in Eq.(S41,S43). They agree well with the numerical  $E_{OBC}$  which is here computed with  $10 \times 10$  lattice sites, with density of states comparison presented later. Bottom) 1D GBZs  $z_x, z_y$  Eq.(S40,S42) for sectors 1 and 2, which traces loops or flattened loops in the complex plane, consistent with the conclusions from Table. I. The two GBZ sectors may look totally different from each other, but they combine to describe the system as a coherent whole. Parameters are  $t_1 = t_2 = t_3 = 1$  and the GBZs are plotted with  $k, k'$  points at intervals of  $\pi/300$ .

► When  $\alpha/\beta = a/b$ , the GBZ and spectrum are given by

$$\text{GBZ} = \left\{ z_{x,1}^{\alpha+\beta}, z_{y,1}^{\alpha+b} = \frac{\sin(\beta b k)}{\sin(a \beta k)} e^{i(a\beta+\beta b)k} \mid k \in \left( -\frac{\pi}{(a+b)\beta}, \frac{\pi}{(a+b)\beta} \right) \right\}, \quad (\text{S49})$$

$$\bar{E}(k) = t_1^{\frac{b}{a+b}} t_3^{\frac{a}{a+b}} \left( \frac{\sin(a+b)\beta k}{\sin a\beta k} \right) \left( \frac{\sin \beta k}{\sin a\beta k} \right)^{-\frac{b}{a+b}} e^{\frac{2i\pi\alpha y'}{a+b}}, \quad (\text{S50})$$

with excellent numerical agreement as shown in FIG. S9.

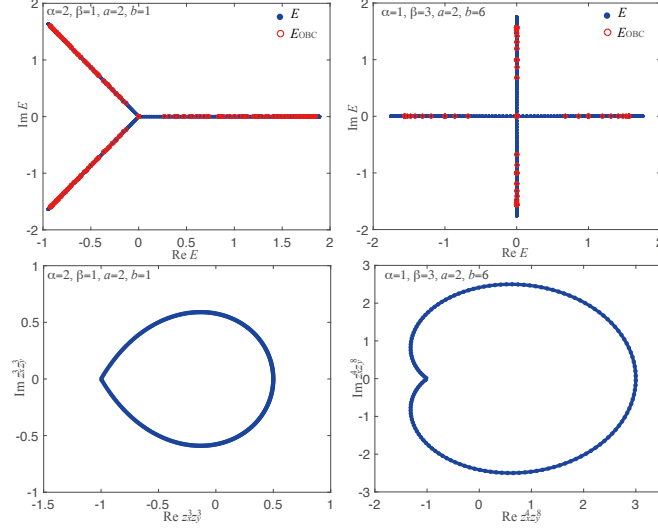


FIG. S9. The constrained GBZs and corresponding spectra  $\bar{E}$  of  $H_{2D, III}$  of two illustrative cases with hopping lengths  $\alpha/\beta = a/b$  as indicated in the panels. Top) Spectrum according to the GBZ (Eq.(S50)), which agree well with the numerical  $E_{\text{OBC}}$  spectrum which is here computed with  $20 \times 20$  lattice sites. Bottom) Corresponding constrained 1D GBZs  $z_x, z_y$  (Eq. (S49)) of these 2D lattices, with cusps that are not present in the GBZs of 1D non-Hermitian lattices. Parameters are  $t_1 = t_2 = t_3 = 1$  and the GBZ is plotted with  $k$  points at intervals of  $\pi/600$ .

- When  $\alpha/\beta < a/b$ , the energy is always zero and  $z_x^{\alpha+\beta} \rightarrow \infty$ ,  $z_y^{\alpha+b} \rightarrow 0$ , which means that the eigenstates always corner-localize, as illustrated in FIG. S10. This is due to non-Bloch collapse, since hoppings  $t_1$  and  $t_3$  do not contain any net component that in the inverse direction of hopping  $t_2$ .

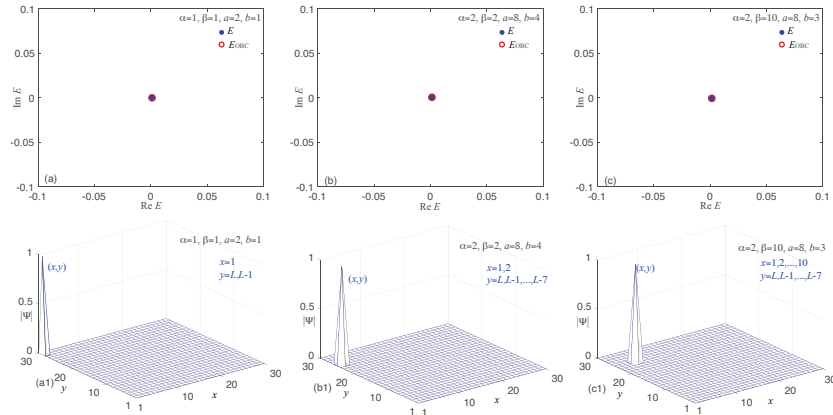


FIG. S10. (Top) Identically zero energies for the case of  $\alpha\beta < a/b$  of the type III system Eq.(S31) ( $\bar{E} = 0$  are from theoretical analysis,  $E_{\text{OBC}} = 0$  are numerical OBC eigenvalues). (Bottom) corresponding corner-localized distribution of eigenstates. The system parameters are  $t_1 = t_2 = t_3 = 1$ , with  $\alpha, \beta, a, b$  indicated in the figures.

*Number of OBC spectral branches for type III hopping lattices*

To find the number of OBC spectral branches for  $H_{2D,III}$  satisfies the symmetry

$$\begin{aligned} U_{v,v'}^{-1} H_{2D,III} U_{v,v'} &= \exp\left(i\frac{2\alpha\pi}{\alpha+\beta}v + i\frac{2a\pi}{a+b}v'\right) H_{2D,III} , \\ U_{v,v'} &= \exp\left(i\frac{2m\pi}{\alpha+\beta}v + i\frac{2n\pi}{a+b}v'\right) |m,n\rangle\langle m,n| , \end{aligned} \quad (S51)$$

with integer indices  $v, v'$  ( $v = 1, 2, \dots, \alpha + \beta$ ,  $v' = 1, 2, \dots, a + b$ ), where  $|m, n\rangle$  are real space basis orbitals.  $U_{v,v'}$  is a unitary operator which satisfies  $U_{v,v'} U_{v,v'}^\dagger = I$ , ('I' represents the unit operator). Assuming that the wave function  $|\Psi^n\rangle$  is an eigenstate of the model Eq.(S31) with eigenvalue  $E_n$ , the other eigenstates  $U_{v,v'}|\Psi^n\rangle$  can be found via symmetry Eq.(S51) with eigenvalue  $\exp\left(i\frac{2\alpha\pi}{\alpha+\beta}v + i\frac{2a\pi}{a+b}v'\right) E_n$ , that is,

$$\begin{aligned} H_{2D,III}|\Psi^n\rangle &= E_n|\Psi^n\rangle , \\ \exp\left(i\frac{2\alpha\pi}{\alpha+\beta}v + i\frac{2a\pi}{a+b}v'\right) H_{2D,III}|\Psi^n\rangle &= \exp\left(i\frac{2\alpha\pi}{\alpha+\beta}v + i\frac{2a\pi}{a+b}v'\right) E_n|\Psi^n\rangle , \\ U_{v,v'}^{-1} H_{2D,III} U_{v,v'}|\Psi^n\rangle &= \exp\left(i\frac{2\alpha\pi}{\alpha+\beta}v + i\frac{2a\pi}{a+b}v'\right) E_n|\Psi^n\rangle , \\ H_{2D,III} U_{v,v'}|\Psi^n\rangle &= \exp\left(i\frac{2\alpha\pi}{\alpha+\beta}v + i\frac{2a\pi}{a+b}v'\right) E_n U_{v,v'}|\Psi^n\rangle . \end{aligned} \quad (S52)$$

Hence we see that the energy spectrum of  $H_{2D,III}$  is parametrized by a 1-parameter family of states, with indices  $v, v'$  taking  $\alpha + \beta, a + b$  possible values. As such, there are

$$\text{LCM}\left[\frac{a+b}{\text{GCD}(a+b, a)}, \frac{\alpha+\beta}{\text{GCD}(\alpha+\beta, \alpha)}\right] , \quad (S53)$$

OBC spectral branches for type III lattices.

## Flowchart of our approach

All in all, the procedure of obtaining the effective BZ and spectrum is illustrated in the following flowchart for generic 2D models. Higher-dimensional models can be dealt with analogously, and will be discussed later.

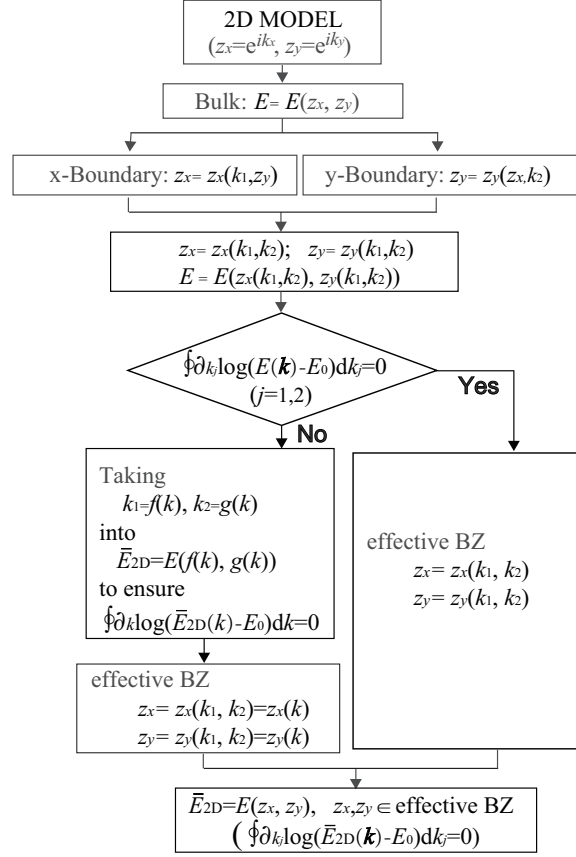


FIG. S11. Flowchart of our approach for generic 2D models. Starting with the original model which can be expressed as  $E(z_x, z_y)$  by identifying  $z_x = e^{ik_x}$ ,  $z_y = e^{ik_y}$ , we find how  $z_x, z_y$  depend on  $k_1, k_2$  by implementing x and y-OBCs separately. If the resulting spectrum does not contain nontrivial spectral winding, the effective BZ is still 2D and we are done. If not, we find 1D parametrizations  $k$  of a submanifold of the  $(k_1, k_2)$  torus such that the spectral windings are trivial. The effective 1D BZ comprises all such 1D paths.

### Density of states in the dimensionally-reduced effective system

In the subsection above, we have shown that in order for the GBZ spectrum of  $H_{2D,III}$  (Eq. S31) to exhibit nonzero winding for any closed path, there is a need to constrain the valid GBZ to a 1D subspace of the original naively obtained 2D GBZ. Here, we show that the numerically obtained OBC spectrum indeed correspond to equally spaced states in the 1D constrained BZ, just like how the momentum eigenstates are distributed in 1D BZ corresponding to a physically 1D system.

To verify that the spectrum of  $H_{2D\text{-red}}$  indeed comprises equally-spaced ‘‘momentum’’ eigenstates, we examine the density of states (DOS) of the OBC spectrum. The DOS is given by

$$\rho(E) = \frac{1}{N} \frac{\delta n}{\delta E}, \quad (\text{S54})$$

which means that there are  $\delta n$  eigenstates in the energy range  $[E, E + \delta E)$  and normalization constant  $N$  is equal to the length of the energy to be measured. What we would like to check is the quantity  $\sigma(k)$ , which is the DOS in momentum space. That is, the momentum range  $[k_i, k_i + \delta k_i)$  ( $i = 1, 2$ ) which corresponds to energy range  $[E, E + \delta E)$  need to be considered, where  $i = 1, 2$  refers to the possible sectors for the GBZs. If the states are indeed uniformly labeled by momentum,  $\sigma_i(k) \propto \rho_i(E) \delta E_i / \delta k$  should be uniform in each sector  $i$ , and  $\sigma(k) = \sum_i \sigma_i(k)$  should only be proportional to the number of sectors corresponding to a particular value of  $k$ . For OBC states predicted by the GBZ sector energies  $\bar{E}_i$ , we have

$$\sigma(k) = \sum_i \sigma_i(k) = \frac{2\pi}{\mathcal{N}} \sum_i \frac{\delta n_i(k)}{\delta E_i(k)} \frac{\delta E_i(k)}{\delta k} = \sum_i \delta n_i(k), \quad (\text{S55})$$

with  $\delta k = 2\pi/\mathcal{N}$ . For each energy interval  $\delta E(k) = \bar{E}_i(k + \delta k) - \bar{E}_i(k)$ , one can obtain the number  $\delta n(k)$  of occupied states within the interval. With the knowledge of the dependence between  $\bar{E}_i$  of the GBZ and momentum  $k$ , it's easy to get the DOS in momentum space  $\sigma(k)$ . This is shown in FIG.S12(a,b) for two illustrative sets of parameters.

#### Model with the GBZ sectors possessing the same energies

For definiteness, we first consider  $H_{2D,III}$  Eq.(S31) with  $\alpha = 2, \beta = 1, a = 1, b = 2$ , such that the energy takes the form

$$E(z_x, z_y) = t_1 z_x^2 z_y + t_2 z_x^{-1} z_y + t_3 z_x^{-1} z_y^{-2}, \quad (\text{S56})$$

where each of  $z_x, z_y$  belongs to the 1D GBZ sectors GBZ<sub>1</sub> and GBZ<sub>2</sub>, which from Sec. Eq.(S46, S47) simplify to

$$\begin{aligned} \text{GBZ}_1 &= \left\{ z_{x,1}^3 = \frac{t_2}{t_1} e^{ik}, z_{y,1}^3 = \frac{t_3}{t_2} \frac{1}{2 \cos(k/3) - 1} \mid k \in [-\pi, \pi) \right\}, \\ \text{GBZ}_2 &= \left\{ z_{x,2}^3 = \frac{t_2}{t_1} (2 \cos(k'/3) - 1), z_{y,2}^3 = \frac{t_3}{t_2} e^{-ik'} \mid k' \in [-\pi, \pi) \right\}, \\ \text{GBZ} &= \text{GBZ}_1 \cup \text{GBZ}_2. \end{aligned} \quad (\text{S57})$$

In other words, the set of GBZ eigenstates consists of eigenstates from both GBZ sectors. The OBC eigenenergies are approximated by GBZ energies, which are given either by  $E(z_{x,1}, z_{y,1}) = \bar{E}_1(k)$  or  $E(z_{x,2}, z_{y,2}) = \bar{E}_2(k')$ , where  $k$  and  $k'$  parametrize their respective GBZs. The GBZ Hamiltonian is hence given by

$$\begin{aligned} H_{2D\text{-red}} &= \bar{H}_{2D,III} = H_1 \oplus H_2, \\ \bar{E}_1(k) = \bar{E}_2(k) &= t_1^{1/3} t_2^{1/3} t_3^{1/3} (2 \cos(k/3) + 1)^{1/3} (2 \cos(2k/3) + 1)^{2/3} e^{2i\pi v/3}, \end{aligned} \quad (\text{S58})$$

with  $k, k' \in (-\pi, \pi]$ ,  $v = 1, 2, 3$ , see FIG. S12(a).  $\bar{E}_1$  and  $\bar{E}_2$  are the corresponding eigenenergies of  $H_1$  and  $H_2$ ; in this case, after substituting the sector-dependent forms of  $z_{x,\nu}$  and  $z_{y,\nu}$ , they happen to take identical functional forms. To justify the integrity of this GBZ construction, we first note that the spectral winding number is zero, since Eq.(S58) is obviously real. Also, both the GBZ<sub>1</sub> and GBZ<sub>2</sub> are period in  $k, k'$ . The correctness of Eq.(S57,S58) is demonstrated in FIG. S8(b), which not only shows that the results of the GBZ and GBZ Hamiltonian can be trusted, but also that the relation between OBC energies and momentum  $k$  are as expected.

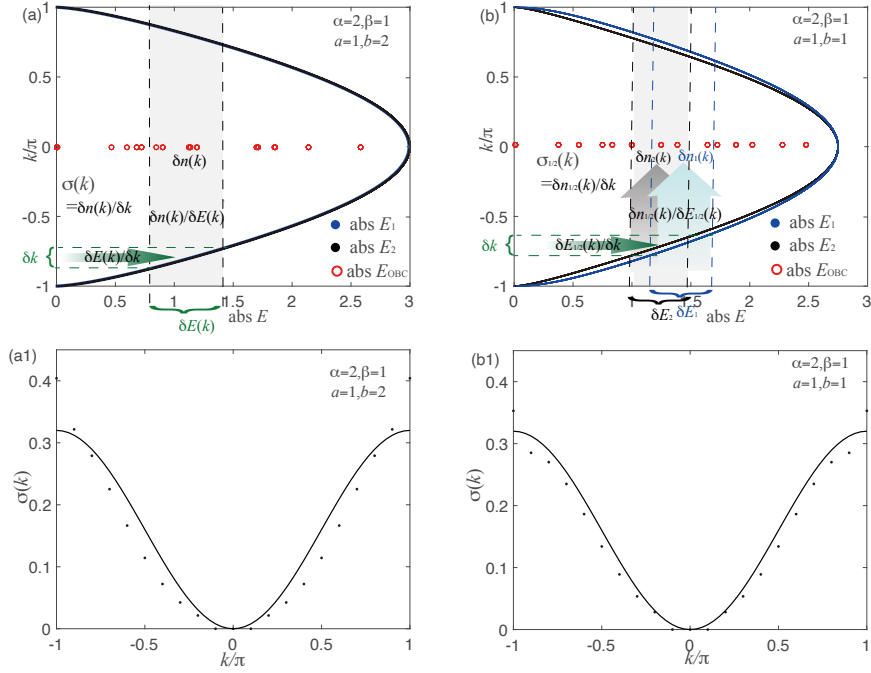


FIG. S12. Density of states (DOS) in momentum space. (a,b) The solid curves denote the dependence of effective 1D GBZ sector energies  $E_1, E_2$  with momentum  $k$  for two possible models Eq.(S32). Numerically, we can obtain  $k \approx k + \delta k$  from each  $\delta E(k)$  point from  $E_{\text{OBC}}$  data (red circles, shown on the central horizontal), and obtain the momentum space DOS  $\sigma(k)$ . (a1,b1) The momentum space DOS profile  $\sigma(k)$  in our model Eq.(S32), with  $\delta k = \pi/8000$ . For both models, the DOS (black dots) can be approximately fitted to a sinusoidal curve (black curve). Parameters are  $t_1 = t_2 = t_3 = 1$ , with a OBC lattice of  $L^2 = 10^2 = 100$  sites.

*Model with the GBZ sectors possessing different energies*

In the above, we considered  $H_{2\text{D,III}}$  (Eq.(S31)) with  $\alpha = b$  and  $\beta = a$ , such that the two 1D GBZ sectors correspond to eigenenergies  $\bar{E}_1$  and  $\bar{E}_2$  Eq.(S58) with equivalent forms. That, however, is not the case for more generic models. Here, we consider an illustrative model with  $\alpha = 2, \beta = 1, a = 1, b = 1$  with dissimilar GBZ eigenenergies for its two sectors. We first write it in terms of  $z_x, z_y$ :

$$E(z_x, z_y) = t_1 z_x^2 z_y + t_2 z_x^{-1} z_y + t_3 z_x^{-1} z_y^{-1}, \quad (\text{S59})$$

where each of  $z_x, z_y$  belongs to either of the two GBZ sectors

$$\begin{aligned} \text{GBZ}_1 &= \left\{ z_{x,1}^3 = \frac{t_2}{t_1} 2 \cos(k/3) e^{ik}, z_{y,1}^3 = \frac{t_3}{t_2} \frac{1}{2 \cos(2k/3) + 1} \mid k \in [-\pi, \pi] \right\}, \\ \text{GBZ}_2 &= \left\{ z_{x,2}^3 = \frac{t_2 \sin(3k'/4)}{t_1 \sin(k'/2)}, z_{y,2}^3 = \frac{t_3}{t_2} \frac{1}{2 \cos(k'/2) + 1} e^{-ik'} \mid k' \in [-\pi, \pi] \right\}, \\ \text{GBZ} &= \text{GBZ}_1 \cup \text{GBZ}_2, \end{aligned} \quad (\text{S60})$$

as introduced in Sec. Eq.(S46, S47). GBZ eigenenergies  $\bar{E}$  take the form of either  $E(z_{x,1}, z_{y,1}) = \bar{E}_1(k)$  or  $E(z_{x,2}, z_{y,2}) = \bar{E}_2(k')$ , with their GBZ Hamiltonian and explicit eigenenergies

$$\begin{aligned} \bar{H}_{2\text{D-red}} &= \bar{H}_{2\text{D,III}} = \bar{H}_1 \oplus \bar{H}_2, \\ \bar{E}_1(k) &= \pm t_1^{1/3} t_2^{1/6} t_3^{1/2} (2 \cos(2k/3) + 1)^{1/2} (2 \cos(k/3))^{2/3} e^{2i\pi v/3}, \\ \bar{E}_2(k') &= \pm t_1^{1/3} t_2^{1/6} t_3^{1/2} (2 \cos(k'/2) + 1)^{1/2} (2 \cos(k'/2))^{2/3} (\sin(k'/4))^{2/3} e^{2i\pi v/3}, \end{aligned} \quad (\text{S61})$$

with  $k, k' \in (-\pi, \pi]$ ,  $v = 1, 2, 3$ , for the model Eq.(S59). As in the previous example, the spectral winding in Eq.(S61) are both zero, and both  $\text{GBZ}_1$  and  $\text{GBZ}_2$  are periodic. However, here  $\bar{E}_1(k)$  and  $\bar{E}_2(k)$  manifestly take different

functional forms. As presented in FIG. S8(a), the numerical results demonstrate the correctness of Eq.(S60,S61), with both  $\bar{E}_1(k)$  and  $\bar{E}_2(k)$  agreeing with the distribution of numerically obtained  $E_{\text{OBC}}$ . Note that strictly, the above GBZ results are exact only in the continuum limit ( $L \rightarrow \infty$ ) where the set of momenta  $k$  tends towards an equally spaced set of points with  $\sim L^{-1}$  separation.

### Circuit simulation of non-Hermitian lattices

Any electrical circuit network can be represented by a graph whose nodes and edges correspond to the circuit junctions and connecting wires/elements. The circuit behavior is fundamentally described by Kirchhoff's law. Non-Hermiticity can be introduced in a RLC electrical circuit by means of negative impedance converters with current inversion (INICs)[63, 64, 68, 131, 134, 141, 156, 157] (Fig. S13(c1)). By means of Kirchhoff's law, it can be shown that [34, 63, 64, 67, 68, 131–134, 136, 138–143, 156–158] each INIC possess the reduced 2-node Laplacian

$$\begin{pmatrix} I'_{\text{in}} \\ I'_{\text{out}} \end{pmatrix} = \frac{1}{2i\omega L} \begin{pmatrix} 1 & -1 \\ 1 & -1 \end{pmatrix} \begin{pmatrix} V_{\text{in}} \\ V_{\text{out}} \end{pmatrix}. \quad (\text{S62})$$

If we further connect an INIC with an inductor of inductance  $2L$  in parallel, we obtain

$$\begin{pmatrix} I_{\text{in}} \\ I_{\text{out}} \end{pmatrix} = \frac{1}{i\omega L} \begin{pmatrix} 1 & -1 \\ 0 & 0 \end{pmatrix} \begin{pmatrix} V_{\text{in}} \\ V_{\text{out}} \end{pmatrix}. \quad (\text{S63})$$

for this parallel configuration pair. This INIC-inductor pair is very versatile, and can be used as the building block of arbitrary non-Hermitian circuit Laplacians. In general, circuit Laplacians  $J$  are obtained via Kirchhoff rule  $\mathbf{I} = J\mathbf{V}$ , where  $\mathbf{I}$  denotes the current input and the voltage  $\mathbf{V}$  measures against ground at each node. As an initial step towards identifying circuits with tight-binding lattice models, we can get  $\mathbf{I} = J\mathbf{V}$  in compact matrix form (Fig. S13(c))

$$\begin{pmatrix} I_1^{m,n} \\ I_2^{m,n} \\ I_3^{m,n} \\ I_4^{m,n} \end{pmatrix} = \begin{pmatrix} -1/(i\omega L_1) & 0 & 0 & 1/(i\omega L_1) \\ 0 & -1/(i\omega L_2) & 0 & 1/(i\omega L_2) \\ 0 & 0 & -1/(i\omega L_3) & 1/(i\omega L_3) \\ 0 & 0 & 0 & i\omega C \end{pmatrix} \begin{pmatrix} V_{m+2,n+1} \\ V_{m-1,n+1} \\ V_{m-1,n-2} \\ V_{m,n} \end{pmatrix}. \quad (\text{S64})$$

For instance, the circuit in Fig. S13 (c), shown for just one unit cell, is mathematically described by a Laplacian matrix, which in momentum space under PBCs, takes the form

$$\begin{aligned} \mathbf{I}(\mathbf{k}) &= J(\mathbf{k})\mathbf{V}(\mathbf{k}), \\ J(\mathbf{k}) &= \mu + t_1 e^{2ik_x + ik_y} + t_2 e^{-ik_x + ik_y} + t_3 e^{-ik_x - 2ik_y}, \end{aligned} \quad (\text{S65})$$

with  $t_j = -1/i\omega L_j$ ,  $j = 1, 2, 3$ , and  $\mu = i\omega C - \sum_{j=1,2,3} t_j$ . This takes the same form as a tight-binding Hamiltonian of the form (FIG. S13(a))

$$H = \sum_{m,n} t_1 |m, n\rangle \langle m+2, n+1| + t_2 |m, n\rangle \langle m-1, n+1| + t_3 |m, n\rangle \langle m-1, n-2|, \quad (\text{S66})$$

with  $H = t_1 e^{2ik_x + ik_y} + t_2 e^{-ik_x + ik_y} + t_3 e^{-ik_x - 2ik_y} = J(\mathbf{k}) - \mu$  when expressed in momentum space.

Notably, the system is sensitive to the boundary orientation, in that the effective lattice takes different forms under different boundary orientations, as shown in FIG. S13 (b1-b3), which correspond to the type I to III models discussed in this work. They correspond to their respective circuits in FIG. S13 (d1-d3).

## 2D MODEL WITH TOPOLOGICAL ZERO MODES FROM 1D TOPOLOGICAL INVARIANT

Here we present a nontrivial implication of the effectively 1D GBZ of our 2D model of the class  $H_{2\text{D},\text{III}}$ . Since the GBZ construction pertains to not just the spectrum, but represents a complex analytic deformation of the Hamiltonian operator itself (to a so-called *surrogate* Hamiltonian, see Ref. [108]), it means that the OBC properties of such Hamiltonians are also nontrivially modified. In particular, an OBC feature of particular interest is the presence of

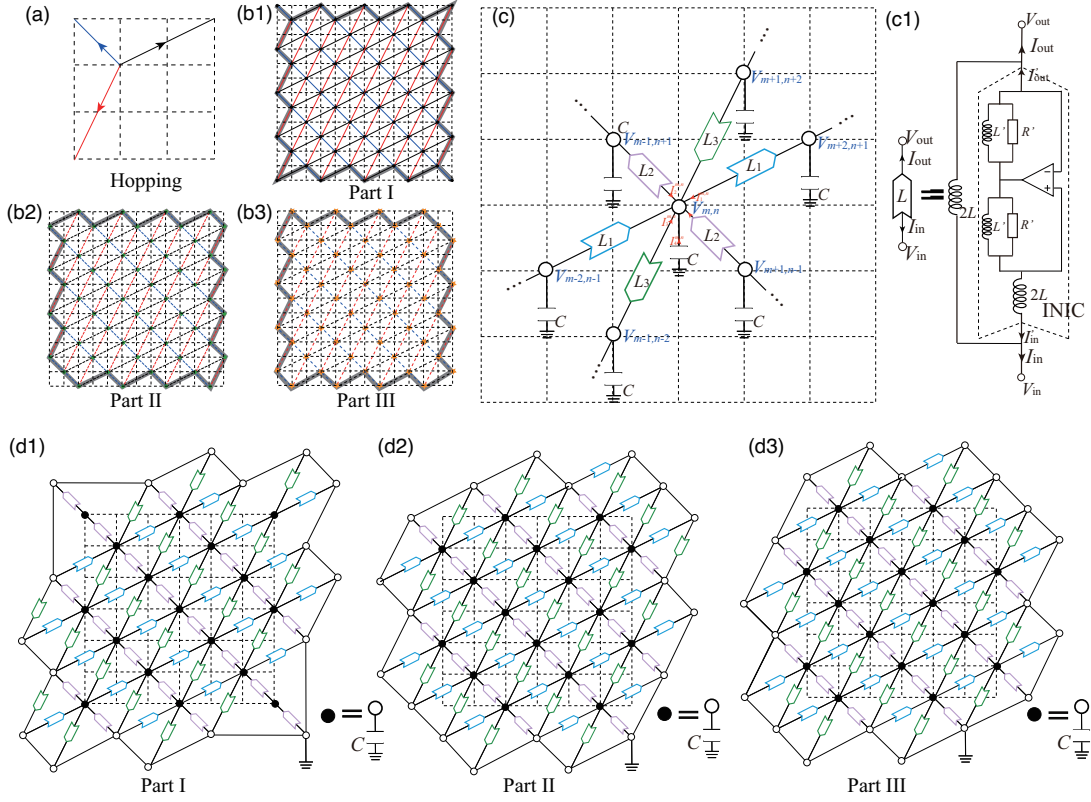


FIG. S13. (a) The three hoppings (black, blue, red) that define the model of Eq.(S66). (b1-b3) Different double OBC boundary orientations on this model lattice gives rise to effective models with hoppings that are oriented differently (labeled as Parts I, II and III). (c) To realize this model with an electrical circuit, each asymmetric hopping can be realized with an INIC  $L_i$ ,  $i = 1, 2, 3$ . (c1) gives the internal make-up of an INIC, with the operation amplifier (triangle) giving rise to the hopping asymmetry. (d1-d3) Circuit realizations of the model variations (b1) to (b3).

topological zero modes. Below, we shall see how our model, which is defined in 2D, nevertheless host topological zero modes defined by a 1D topological invariant.

Noting that the GBZ construction is completely determined by the characteristic polynomial (bulk energy dispersion), we can construct a 2-band topological Hamiltonian with a 1D constrained GBZ by writing down a model with exactly the same eigenenergy dispersion as Eq.(S32) up to a constant offset  $c$  that gaps the system, i.e.

$$H = \begin{pmatrix} 0 & H_{12} \\ H_{21} & 0 \end{pmatrix}, \quad (\text{S67})$$

with eigenenergies  $\mathcal{E}_{1,2}$ , which are stipulated to satisfy  $(\mathcal{E}_{1,2})^2 = H_{12}H_{21} = E + c = t_1 z_x^\alpha z_y^a + t_2 z_x^{-\beta} z_y^a + t_3 z_x^{-\beta} z_y^{-b} + c$ , and

$$\begin{aligned} H_{12} &= (E + c)/Z = (t_1 z_x^\alpha z_y^a + t_2 z_x^{-\beta} z_y^a + t_3 z_x^{-\beta} z_y^{-b} + c)/Z, \\ H_{21} &= Z, \end{aligned} \quad (\text{S68})$$

where we allow  $Z$  to assume either of the two forms for illustrative purposes:  $Z = z_y^a$  or  $Z = z_x^{-\beta}$ .  $E$  is the energy function of Eq.S32. The gap induced by  $c$  does not affect the GBZ solutions since energy degeneracies are not sensitive to a constant offset.

First, for the model Eq.(S31) with OBCs, either along one or both boundary directions, the spectrum of the GBZ hamiltonian must have a net zero winding number, even though the winding number of the off-diagonal term  $H_{12}$  is dependent on the  $Z$  term.

With  $\alpha/\beta > a/b$ , its GBZ Hamiltonian takes the form

$$\bar{H} = \bar{H}_1 \oplus \bar{H}_2 = \begin{pmatrix} 0 & \bar{H}_{12} \\ \bar{H}_{21} & 0 \end{pmatrix} = \begin{pmatrix} 0 & \bar{H}_{12}^1 \\ \bar{H}_{21}^1 & 0 \end{pmatrix} \oplus \begin{pmatrix} 0 & \bar{H}_{12}^2 \\ \bar{H}_{21}^2 & 0 \end{pmatrix}, \quad (\text{S69})$$

$$\bar{H}_{12}^i = (\bar{E}_i + c)/Z_i, \quad \bar{H}_{21}^i = Z_i. \quad (\text{S70})$$

with  $\bar{E}_i = \bar{H}_{12}^i \bar{H}_{21}^i$ , ( $i = 1, 2$ ) Eq.(S41,S43). Both  $\bar{H}_{12}^i$ ,  $i = 1, 2$  have the same forms of  $z_{x,i}, z_{y,i}$ :

$$\begin{aligned} z_{x,1}^{\alpha+\beta} &= \frac{t_2 \sin((a+b)\beta k)}{t_1 \sin((\alpha b - a\beta)k)} e^{i(\alpha b + \beta b)k}, & z_{y,1}^{\alpha+\beta} &= \frac{t_3 \sin(\beta b k) \sin((\alpha b - a\beta)k)}{t_2 \sin(a\beta k) \sin((\alpha b + \beta b)k)}, & k &\in \left[ -\frac{\pi}{(\alpha + \beta)b}, \frac{\pi}{(\alpha + \beta)b} \right], \\ z_{x,2}^{\alpha+\beta} &= \frac{t_2 \sin(\beta a k') \sin((\alpha a + \alpha b)k')}{t_1 \sin(\alpha \alpha k') \sin((\alpha b - \beta a)k')}, & z_{y,2}^{\alpha+\beta} &= \frac{t_3 \sin((\alpha b - a\beta)k')}{t_2 \sin((\alpha a + a\beta)k')} e^{i(\alpha a + \alpha b)k'}, & k' &\in \left[ -\frac{\pi}{\alpha(a+b)}, \frac{\pi}{\alpha(a+b)} \right], \end{aligned} \quad (\text{S71})$$

For each GBZ sector  $i$ , we have  $Z_i = z_{y,i}^a$  or  $Z_i = z_{x,i}^{-\beta}$  depending on the choice of illustrative example. Since we have designed this model such that it harbors nontrivial topological zero modes under double OBCs, from established results [85], both  $\bar{H}_{12}$  and  $\bar{H}_{21}$  must have nonzero winding about  $E = 0$  (we shall suppress the GBZ sector label  $i$  unless it is explicitly referred to), and these windings sum to zero. For the off-diagonal term  $\bar{H}_{12}$ , the winding number about  $E = 0$

$$\omega(\bar{H}_{12}) = \oint dk \partial_k \log \bar{H}_{12} = \omega(\bar{H}_{12}^1) + \omega(\bar{H}_{12}^2) \neq 0, \quad (\text{S72})$$

is also nonzero. We emphasize that although this nonzero winding criterion for topological modes was originally formulated for a 1D system, we have now used it for the 1D effective GBZ of a *physically* 2D system. Some examples of cases with topological zero modes for double OBCs but not single OBCs are given in Fig. S14.

However, this model with a single OBC exhibit very different results. If we choose  $Z = z_y^a$ , only when the  $\mathbf{x}$  PBC,  $\mathbf{y}$  OBC, the system has topological zero modes, the winding number of  $\bar{H}_{12}$  is non-zero on the single OBC GBZ. By contrast, the same system with  $\mathbf{x}$  OBC,  $\mathbf{y}$  PBC has no topological zero modes (Fig. S14). With double OBCs, the 1D GBZ for the double OBCs give rise to zero winding number for  $\bar{H}_{12}^1$ , and nonzero winding number for  $\bar{H}_{12}^2$ , both summing to a nonzero total winding of  $\bar{H}_2$  from Eq. S69.

If we choose  $Z = z_x^{-\beta}$  instead, the opposite is the case, the system with  $\mathbf{x}$  OBC,  $\mathbf{y}$  PBC have topological zero modes, the system with  $\mathbf{x}$  PBC,  $\mathbf{y}$  OBC does not have. The winding number of  $\bar{H}_{12}^1$  is non-zero, the winding number of  $\bar{H}_{12}^2$  is zero in the GBZ Hamiltonian with double OBC. In an analogous way, the 2D model with double OBC also has topological zero modes which is contributed by  $\bar{H}_1(k)$  from Eq.S69.

We demonstrate the above arguments for two illustrative cases of  $\alpha, \beta, a, b$  parameters. We use  $Z = z_y$  and examine the energy spectrum of our 2D two-band model Eq.S67 with different boundary conditions. The observed numerical results prove the correctness of the above theoretically established results, in FIG. S14,S15. Specifically, it demonstrates that the construction of the effective 1D GBZ Hamiltonian can correctly predict the topological zero mode, despite the system being physically a 2D system.

## GENERALIZATIONS TO HIGHER DIMENSIONS

Our approach for getting the correct 2D GBZs as well as their 1D constrained GBZs, if necessary, can be generalized to higher dimensions. In generic number of dimensions, the GBZ will first be symmetrically constructed in terms of relations between complex  $z_x, z_y, z_z, \dots$  and real  $k_1, k_2, k_3, \dots$ . If there exist nonzero spectral windings, they will also have to be constrained to a lower dimension such that the all spectral windings in the constrained GBZ become zero. Specializing to 3 dimensions for definiteness (higher dimension cases can be analogously written down), suppose we have

$$H_{3D} = \sum_{m,n,l} \sum_{a,b,c} t_{abc} |m, n, l\rangle \langle m + a, n + b, l + c|, \quad (\text{S73})$$

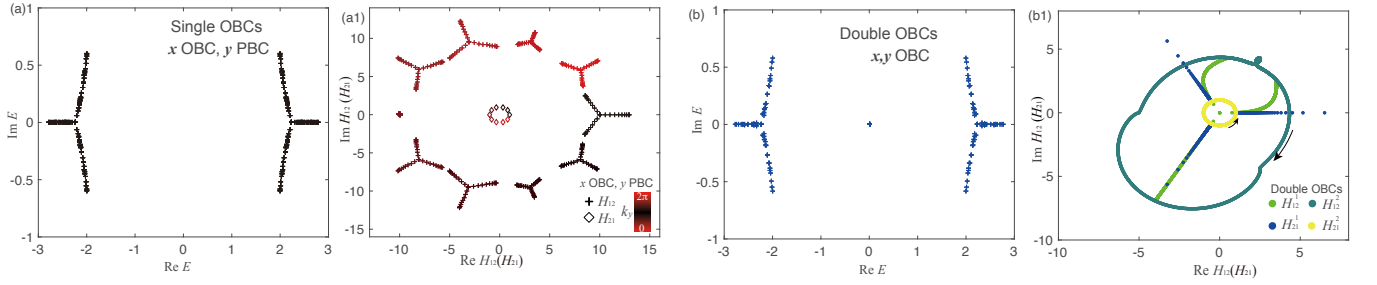


FIG. S14. Energy spectrum of the 2-band model (Eq.(S67)) with (a) single OBCs and (b) double OBCs, showing double OBC topological modes that originate from a 1D topological invariant. We have  $Z = z_y$ ,  $\alpha = 2, \beta = 1, a = 1, b = 2$ , and the constant is set to  $c = 5$  to make sure that the 2-band model is gapped under PBC. In (a), there is no topological zero mode, which is corroborated by the fact that  $H_{12}$  in (a1) has zero winding. In (b), the presence of a double OBC topological zero mode agrees with the fact that for each of  $H_{12}^i$  and  $H_{21}^i$ , the sum of their windings over  $i = 1, 2$  is nonzero. The winding of  $H_{12}^2$  is  $\omega(H_{12}^2) = -1 = -\omega(H_{21}^2)$  and  $\omega(H_{12}^1) = \omega(H_{21}^1) = 0$ . Note that for the single OBC (xOBC, yPBC) case, the winding is about  $k_x$ , not  $k_y$ , so the winding of  $H_{12}$  and  $H_{21}$  is zero. The plots are generated with (a)  $k_y = -\pi : \pi/30 : \pi$ ,  $L = 10$ , (b) with  $L_x = L_y = 10$ .

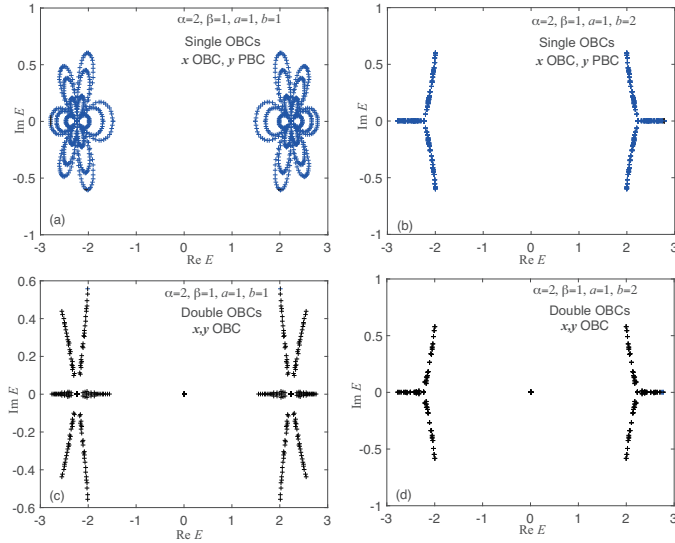


FIG. S15. Energy spectrum of the 2-band model (Eq.(S67)) with  $Z = z_y$ , under single and double open boundary conditions. The Left and Right columns denote different sets of parameters (Marked in the figure). Evidently, under double OBCs, we observe topological zero modes that originate from a 1D topological invariant, indicating that the GBZ is an effective 1D GBZ, not a 2D GBZ. The constant offset in Eq.(S67) is set to  $c = 5$  to make sure that the 2-band model is gapped under PBCs. The system is numerically discretized such that (a,b)  $k_y = -\pi : \pi/30 : \pi$ ,  $L_x = 10$ , (c,d)  $L_x = L_y = 10$ .

with hopping amplitudes  $t_{abc}$  and  $a, b, c$  generic integers which represent hopping directions and distances. In the same way as before, we insert the ansatz  $|\psi\rangle \propto \sum_{m,n,l} \psi_{mnl} |m, n, l\rangle$  with  $\psi_{m,n,l} = z_x^m z_y^n z_z^l$  into the bulk equations to obtain

$$E(z_x, z_y, z_z) = \sum_{a,b,c} t_{abc} z_x^a z_y^b z_z^c. \quad (\text{S74})$$

Like before, there are generally many sets of  $(z_x, z_y, z_z)$  that corresponds to a particular energy  $\bar{E} = E(z_x, z_y, z_z)$ .

To incorporate the boundary conditions, we can express a wavefunction  $|\Psi\rangle$  with eigenenergy  $\bar{E} = E(z_x, z_y, z_z)$  as

different 1D chains in the  $x, y$  or  $z$ -directions, with two other momenta as parameters:

$$\begin{aligned}
|\Psi\rangle &= |\Psi^1\rangle = |\Psi^2\rangle = |\Psi^3\rangle = \propto \sum_{m,n,l} \Psi_{mnl} |m, n, l\rangle, \\
\Psi_{mnl} &= \Psi_{mnl}^1 = \Psi_{mnl}^2 = \Psi_{mnl}^3, \\
\Psi_{mn}^1 &= \sum_{z_y, z_z} \left( \sum_j f_{z_x, j} z_{x, j}^m \right) g_{z_y} z_y^n h_{z_z} z_z^l, \\
\Psi_{mnl}^2 &= \sum_{z_x, z_z} f_{z_x} z_x^m \left( \sum_{j'} g_{z_y, j'} z_{y, j'}^n \right) h_{z_z} z_z^l, \\
\Psi_{mnl}^3 &= \sum_{z_x, z_y} f_{z_x} z_x^m g_{z_y} z_y^n \left( \sum_{j''} h_{z_z, j''} z_{z, j''}^l \right).
\end{aligned} \tag{S75}$$

Here  $|\Psi^1\rangle$ ,  $|\Psi^2\rangle$ ,  $|\Psi^3\rangle$  are different direction decompositions of the same wave function  $|\Psi\rangle$ , and the first summation in the equation  $\Psi_{mnl}^j$ ,  $j = 1, 2, 3$  means we must consider all the sets  $z_x, z_y, z_z$  which have same energy  $\bar{E}$ .

Taking the different manifestations of the wave function  $|\Psi\rangle$  into the boundary conditions along different directions (i.e.,  $\mathbf{x}, \mathbf{y}, \mathbf{z}$  direction), like boundary conditions along  $\mathbf{x}$  direction, we have  $\Psi_{m'n} = \Psi_{m'n}^1 = 0$  with special value  $m'$  and any values  $n$ , like '1D' system with parameters  $z_y, z_z$ . Thus, for a particular fixed energy, we can in general write down a relation between  $z_x$  and  $z_y, z_z$ , i.e.

$$\mathcal{F}_1(z_x, z_y, z_z, k_1) = 0, \tag{S76}$$

with real  $k_1$  "momentum" parametrizing one direction in the GBZ. In the same way, we can get other relations along  $\mathbf{y}, \mathbf{z}$  directions

$$\mathcal{F}_2(z_x, z_y, z_z, k_2) = 0, \tag{S77}$$

$$\mathcal{F}_3(z_x, z_y, z_z, k_3) = 0, \tag{S78}$$

with real  $k_2, k_3$ . By construction, the  $z_x, z_y, z_z$  satisfy all the boundary conditions. Hence we have 3 unknowns  $z_x, z_y, z_z$  with 3 independent relational equation (Eq. S76, S77, S78), which can in principle be simultaneously solved to yield relations

$$z_i = \mathcal{F}_i(k_1, k_2, k_3), \tag{S79}$$

with  $i = x, y, z$ . Taking  $z_x, z_y, z_z$  Eq.(S79) into the energy equation Eq.(S74), we can equivalently get the GBZ-predicted OBC energy

$$E(z_x, z_y, z_z) = \bar{E}(k_1, k_2, k_3). \tag{S80}$$

If the winding number of  $\bar{E}(k_1, k_2, k_3)$  Eq.(S74) is zero for all closed loops, the resultant GBZ of the 3D system will just be given by

$$\text{GBZ}_{3\text{D}} = \{z_x, z_y, z_z | z_i = \mathcal{F}_i(k_1, k_2, k_3), i = x, y, z\}. \tag{S81}$$

And if the spectral winding number of  $E(k_1, k_2, k_3)$  Eq.(S80) is non-zero, we must determine what constraints we need on the parameters  $k_1, k_2$  and  $k_3$  such that the spectral winding of all possible paths is zero, and that the GBZs defined by  $z_x, z_y, z_z$  are periodic as we vary any of the remaining  $k_i$ . The explicit construction of such constraints to obtain the correct GBZ depends on the model, and will be the subject of future work - in the next subsection, we give a minimal example in 3D. In general, the constraints can either reduce the correct GBZ to a 2D subspace, or even a 1D subspace.

*Illustrative simple 3D model*

For a minimal example of the GBZ construction of a 3D model, we consider 2 hopping terms in 3D space i.e.

$$H_{3D} = \sum_{m,n,l} t_{abc} |m, n, l\rangle \langle m+a, n+b, l+c| + t_{a'b'c'} |m, n, l\rangle \langle m-a', n-b', l-c'|, \quad (\text{S82})$$

with real  $a, b, c, a', b', c'$ . Assuming the wave function ansatz  $|\psi\rangle \propto \sum_{m,n,l} \psi_{mnl} |m, n, l\rangle$  with  $\psi_{m,n,l} = z_x^m z_y^n z_z^l$ , we arrive at two possible cases. In the first case,  $a/a' = b/b' = c/c'$  and previous derivations can be straightforwardly generalized to give

$$\text{GBZ}_{3D} = \left\{ z_x^{a+a'} z_y^{b+b'} z_z^{c+c'} = \frac{t_{a'b'c'} \sin(a'k)}{t_{abc} \sin(ak)} e^{i(a+a')k} \mid k \in \left( -\frac{\pi}{a+a'}, \frac{\pi}{a+a'} \right] \right\}, \quad (\text{S83})$$

$$E(z_x, z_y, z_z) = E(k) = \left( \frac{t_{abc}^a t_{a'b'c'}^a}{(\sin(ak))^a (\sin(a'k))^a} \right)^{\frac{1}{a+a'}} \sin((a+a')k) e^{\frac{2i\pi a y}{a+a'}},$$

with  $E(z_x, z_y, z_z) = t_{abc} z_x^a z_y^b z_z^c + t_{a'b'c'} z_x^{-a'} z_y^{-b'} z_z^{-c'}$ , as shown in FIG. S16 (b,b1,c,c1). In this model Eq.(S83) with  $a/a' = b/b' = c/c'$ , the GBZ is only determined by a condition on the combination  $z_x^{a+a'} z_y^{b+b'} z_z^{c+c'}$  rather than  $z_x, z_y$  and  $z_z$  separately, and is akin to a 1D model along the  $a\mathbf{x} + b\mathbf{y} + c\mathbf{z}$  direction, which is consistent with the results of numerical diagonalization, as in FIG. S3(a1—a3).

In the other case where  $a/a' = b/b' = c/c'$  does not hold, there is non-Bloch collapse due to uncompensated hoppings in certain directions, and the GBZ and energy are simply given by

$$\text{GBZ} = \left\{ z_x^{a+a'} z_y^{b+b'} z_z^{c+c'} = -1 \right\}, \quad (\text{S84})$$

$$E(z_x, z_y, z_z) = 0,$$

as shown in FIG. S16 (a,a1). In both of these cases, the GBZ spectrum have zero winding number, and further dimensional reduction is not necessary.

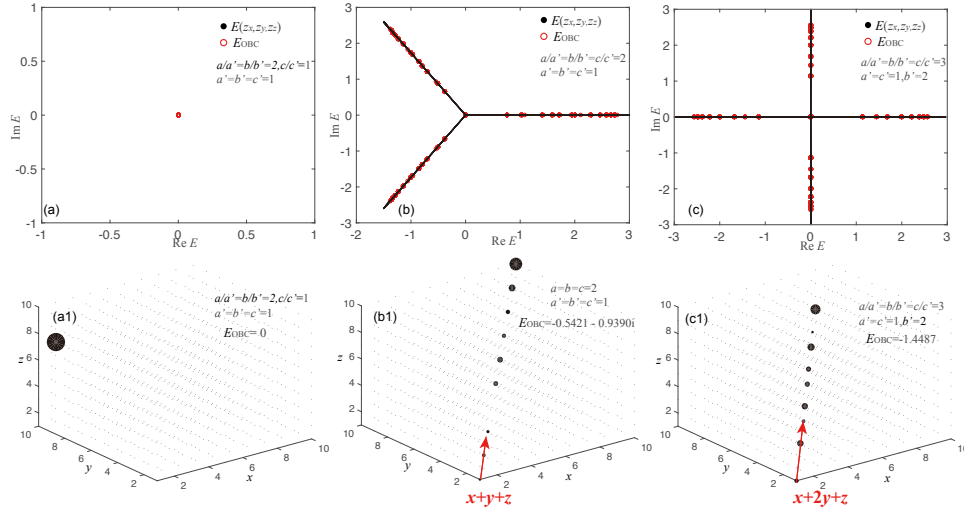


FIG. S16. Spectra and illustrative eigenstates for  $H_{3D}$  with different  $a, b, c, a', b', c'$  case. (a–c) Excellent agreement between the GBZ eigenenergies  $E(z_x, z_y)$  of GBZ and OBC eigenenergies  $E_{\text{OBC}}$  of Eq.(S82). (a1–c1) Spatial profiles for the  $E_{\text{OBC}}$  eigenstate of a few other illustrative cases, clearly showing that the skin states are aligned along the  $(a\mathbf{x} + b\mathbf{y} + c\mathbf{z})$  direction (b1,c1). The model parameters are  $L_x = L_y = L_z = 10$ ,  $t_{abc} = 1$ ,  $t_{a'b'c'} = 2$  and the specific values of  $a, b, c, a', b', c'$  and  $E_{\text{OBC}}$  are indicated in the figure.

In general, in arbitrarily high dimensional systems, the number of independent  $z_i$  is always the same as the number of independent relations  $\mathcal{F}_i$ , with zero spectral winding either automatically satisfied or fulfilled via dimensional reduction to a lower-dimensional GBZ.

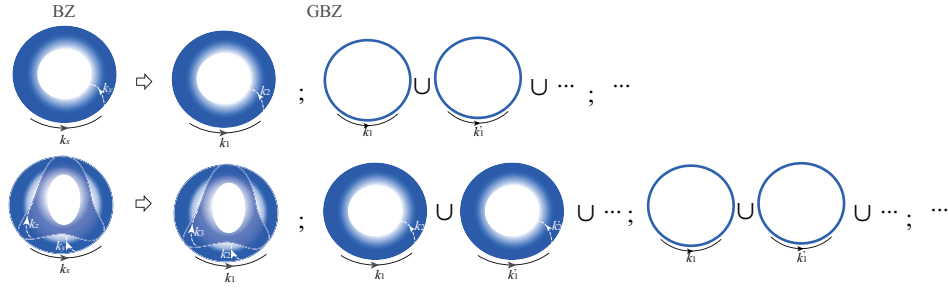


FIG. S17. Schematic illustration of effective BZ for higher dimensional systems. (Top) In 2D lattices that are Hermitian or “unentangled”, the BZ is simply a 2D torus; yet for “entangled” non-Hermitian cases, the effective BZ becomes the union of one or more 1D tori. (Bottom) Similarly, 3D lattices that are Hermitian or “unentangled” have 3D tori as their BZ, but for “entangled” non-Hermitian cases, the effective BZ is in general a union of various 1D and 2D tori.